Lawrence Berkeley National Laboratory

LBL Publications

Title

Ionic Liquid Engineering in Perovskite Photovoltaics

Permalink

Journal

ISSN

Authors

Wang, Fei
Duan, Dawei
Singh, Mriganka
et al.

Publication Date

DOI

Copyright Information

Peer reviewed

Ionic Liquid Engineering in Perovskite Photovoltaics

Fei Wang, Dawei Duan, Mriganka Singh, Carolin M. Sutter-Fella, Haoran Lin, Liang Li*, Panče Naumov*, and Hanlin Hu*

F. Wang, D. Duan, Prof. H. Lin, Prof. H. Hu

Hoffman Institute of Advanced Materials, Shenzhen Polytechnic, Shenzhen, China

E-mail: hanlinhu@szptu.edu.cn (H. H.)

Dr. M. Singh, Dr. C. M. Sutter-Fella

Molecular Foundry Division, Lawrence Berkeley National Laboratory, Berkeley, California 94720, United States

Prof. L. Li

Department of Sciences and Engineering, Sorbonne University Abu Dhabi, Abu Dhabi, United Arab Emirates

Email: liang.li@sorbonne.ae (L. L.)

Prof. L. Li, Prof. P. Naumov

Smart Materials Lab, New York University Abu Dhabi, Abu Dhabi, United Arab Emirates

Prof. P. Naumov

Molecular Design Institute, Department of Chemistry, New York University, 100 Washington Square East, New York, United States

Email: pance.naumov@nyu.edu (P. N.)

Abstract: Over the past decade, perovskite photovoltaics have approached other currently available technologies and proven to be the most prospective type of solar cells. Although the many-sided research in this very active field has generated consistent results with regards to their undisputed consistently increasing power conversion efficiency, it also produced several rather contradictory opinions. Among other important details, debate surrounding their proneness to surface degradation and poor mechanical robustness, as well as the environmental footprint of this materials class remains a moot point. The application of ionic liquids appears as one of the potential remedies to some of these challenges due to their high conductivity, the opportunities for chemical 'tuning' of the structure, and relatively lower environmental footprint. This article provides an overview, classification, and applications of ionic liquids in perovskite solar cells. We summarize the use and role of ionic liquids as versatile additives, solvents, and modifiers in perovskite precursor solution, charge transport layer, as well as for interfacial and stability engineering. Finally, challenges and the future prospects for the design and/or selection of ionic liquids with a specific profile that meets the requirements for next generation highly efficient and stable perovskite solar cells are proposed.

1. Introduction

Over the past decade Hybrid organic-inorganic perovskite solar cells (PSCs) have drawn much research interest on account of their tunable bandgap, long charge carrier, incremental power conversion efficiencies (PCEs), and simple preparation.[1–3][4] At the state-of-the-art of this field, thanks to the optimization of the chemical composition and an appropriate device structure, a PCE efficiency increase over 25%, brings these materials closer to the requirements for mass production of perovskite-based photovoltaic devices.[5–7] This performance, however, is outset by valid concerns over the chemical stability and decreased efficiency of the perovskite materials over time, among other challenges such as mechanical properties and environmental footprint. These concerns have inspired extensive research and device design efforts that include component engineering, additive engineering, interface engineering and solvent engineering to attain control over both the synthesis of the perovskites, as well as over the later stage of optimization of the perovskite-based devices.[8–11] Nevertheless, the optimal combination of efficiency and stability in high-quality perovskite devices remains to be addressed.

Additives can affect structure and morpology of the bulk material, and provide an alternative approach that does not require susbtantial change in methodology. This line of thought has resulted in incorporation of additives to control the formation of perovskite films, and include polymers, nanoparticles, Lewis acids or bases, fullerene derivatives, salts, 2D material, and low-dimensional perovskites.[12,13] Recently, Zhu et al. have demonstrated that Lewis bases added to the perovskite precursor solution lead to favorable interactions with the Pb^{2+} and FA^+ cations in the perovskite crystals. This effectively improves the quality of the perovskite films, as concluded from the retention of 90% of the original performance of the devices after 1,000 h at 80 °C, reaching to an efficiency of 22.43%.[14] The additives not only affect the quality of the film, but they can also be used as interface modification layer, electron transport (ETL) and hole transport layers (HTL) to remedy interface defects, restrain nonradiative recombination, and improve charge transport.[15] You et al. reproted surface defect passivation of the organic halide salt phenethylammonium iodide (PEAI)inn perovskite films and perovskite solar cells with a confirmed PCE of 23.32%.[16] Turren-Cruz and colleagues employed phenyl-C_{61}-butyric acid methyl ester (PCBM) and poly(methyl methacrylate) (PMMA) to embellish the ETL/perovskite and the HTL/perovskite interface which passivates the perovskite and reduces recombination.[17] However, as many of these functional materials are toxic or complex to prepare, the search for green, environmentally beningn, cost-effective and efficient materials continues to apply additive, interface, and stability engineering to perovskites.[18,19]

Ionic liquids (ILs), a class of molten salts that exist as liquids at room temperature, are one of the most prospective materials as additives to perovskite solar cells.[20–22] The cations can be selected across a range mainly pyridinium, imidazolium[23,24] and quaternary ammonium cations[25] or their derivatives, while the anions can be halides (X^-),[26] formate ($HCOO^-$),[27,28] acetate (CH_3COO^-),[29,30] hexafluorophosphate ions (PF_6^-),[31,32] and tetrafluoroborate (BF_4^-).[33] The structures of some common cations and anions of ILs are shown in Figure 1. Different from the traditional inorganic salts, the size difference between the cation and the anion in ionic liquids is substantial which translates into weaker attractive electrostatic forces, and as a result, lower melting point which is usually below room temperature. The other salient features of the ionic liquids are that they can be considered "green" and environmentally friendly mainly owing to the non-volatile characteristics. In addition, due to the diversity of

3

anions and cations of ILs and the deep identification of the toxicity composition of ILs, we can avoid the toxic components to design the ILs with non-toxic components for perovskite devices.[34] These features become particularly relevant when these materials are compared against the traditional organic solvents, additives and passivators applied in perovskite solar cells.[35,36] Given the concerns with the metal (Pb) content of the standard PSCs, this idea has been translated to replace toxic organic solvents in these materials. Moreover, halogen defects caused by halogen ion migration in perovskite can usually be occupied by ILs due to the rich electron density of ILs, which suggest the great potential of ILs in inhibiting ion migration in perovskite.[37] Some of the benefits of ionic liquids are the wide liquid range, high carrier mobility, and importantly, thermal and electrochemical stability. Taking the advantages of designed structure of ILs with functional groups, the opportunities for the interactions (hydrogen bonding, coordination, electrostatic interaction) between the ILs and perovskite material are important to improve the crystallization propensity for the acquisition of high-quality film with less defects, which cooperate with hydrophobic groups in designed ILs to enhance water insensitivity of the respective films.[38] Based on these excellent properties, various ILs have been introduced into perovskites and highly efficient, stable perovskite solar cells have been demonstrated.[39,40]

In this review, we summarize the latest progress in the application of ILs in PSCs and elaborate the specifics of the role of ILs in perovskite solar cells and the underlying mechanisms, aimed to advance further and to stimulate research into preparation of efficient and stable ILs-containing perovskite optoelectronic devices. We present the effect of different and large amounts of ILs on PSCs in engineering of the perovskite precursors, charge transport layer, interface, and stability. An outlook on possible future developments of the application of ILs in the perovskite field is also provided, and discussed.
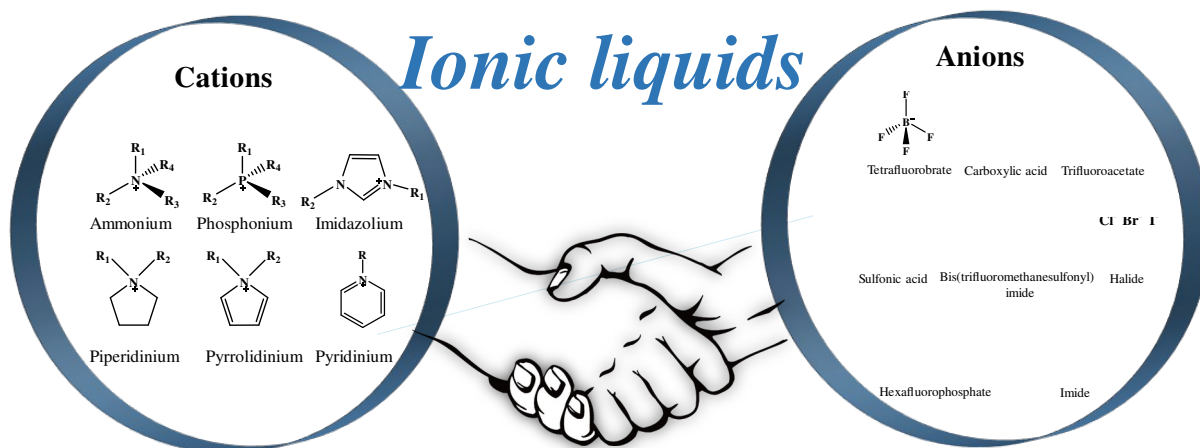
Figure 1. The structure of some common cations and anions of ILs in perovskite solar cells field.

2. Perovskite precursor solution engineering with ionic liquids

### 2.1. Challenges with the perovskite film morphology

As indicated above, PSCs of high efficiency and stability were prepared by optimizing the perovskite precursor solution engineering, interfacial engineering, and device structure.[41] Since the main component in a solar cell, at least from the materials perspective, is the perovskite film, the preparation of high-quality perovskite films has been the main focos of plethora of studies aimed to increase the efficiency of the PSC devices. Several methods have been proposed to prepare a high-quality perovskite layer, and these include spin-coating, two-step sequential deposition, blade coating, and vacuum vapor deposition.[42] Even though the preparation process has been greatly improved, these methods result in significant concentration of few defects and consequently, in reduced efficiency.

2.2. Ionic liquids as additives in perovskite precursor solutions

Additives or solvents in the perovskite precursor solution have been widely investigated and it has been evidenced they can significantly influence the perovskite crystal growth and film morphology.[43] In this context, being a "green additive", ILs have a proven record of beneficial effects in the perovskite precursor solution engineering to control the crystalline properties and surface morphology (Table 1). ILs can be used in the spin-coated films or occured chemical action with elements in perovskite precursor solution, which affects the

crystal growth of the perovskite and usually results in larger crystalline domains and highly heterogeneous film. Specifically, ILs contained functional groups, including the hydrogen bond acceptor/donor or lone pair electrons, which promote the formation of the hydrogen bonds with MA(FA)X and adducts with PbX_2. These interactions induced the emergence of the intermediate phase, thus the ILs are able to control the crystallization process of perovskite through the intermediate phase.[19] Seo et al.[44] reported that 5% (mol) methylammonium formate (MAFa) in the perovskite precursor solution affords larger crystalline domains, which correlates with the more effective charge collection and excellent photovoltaic performance. These effects were attributed to coordination between $HCOO^-$ and Pb^{2+} that is expected to affect the crystal growth. The suggested mechanism is thought to be composed of three steps (Figure 2a). In the first step, Pb^{2+} is coordinated by $HCOO^-$ to form the ion pair $HCOO^--Pb^{2+}$. This is followed by the second step, where the $Pb^{2+}-I^-$ gradually replaces $HCOO^--Pb^{2+}$ during annealing at 100 °C. In the third step, the complex $HCOO^--Pb^{2+}$ is entirely replaced by $Pb^{2+}-I^-$ to facilitate the growth of the perovskite crystal. The images of the perovskite film collected during the annealing (Figure 2b) and the respective scanning electron microscopy (SEM) images (Figure 2c) suggest that the crystal growth is slowed down by the presence of MAFa, resulting in increase in the average grain sizes from 170 to 325 nm upon addition of MAFa. Such high-quality perovskite films showed power conversion efficiency of 19.5%.

Similarly, Zhang et al.[45] incorporated functionalized imidazolium ionic liquids modified with $-CH_2-CH=CH_2$ (CC2), $-CH_2C \equiv CH$ (CC3) and $-CH_2 \equiv CN$ (CN) groups in $CH_3NH_3PbI_3$-type perovskites to improve the quality of the perovskite layers. SEM images showed a better coverage and uniformity of the IL-doped films compared to the reference (Figure 2d). Ils CC2, CC3, and CN in reaction with PbI_2 formed the corresponding $(CC2)PbI_3$, $(CC3)PbI_3$, and $(CN)PbI_3$ salts with characteristic 1D PbI_3^- chains (Figure 2e). However, the closest I–I and Pb–I distances depend on the IL used, and this has an effect on the crystal growth and solubulity. $(CC2)PbI_3$ was easier to dissolve in DMSO than the other salts. The imidazolium cations and the PbI_3^- anion in $(CC2)PbI_3$ formed six hyrogen bonds, contrary to the four hydrogen bonds in $(CC3)PbI_3$ and $(CN)PbI_3$. The corresponding PSCs doped with IL CC2 salt showed the highest PCE of 19.21%.
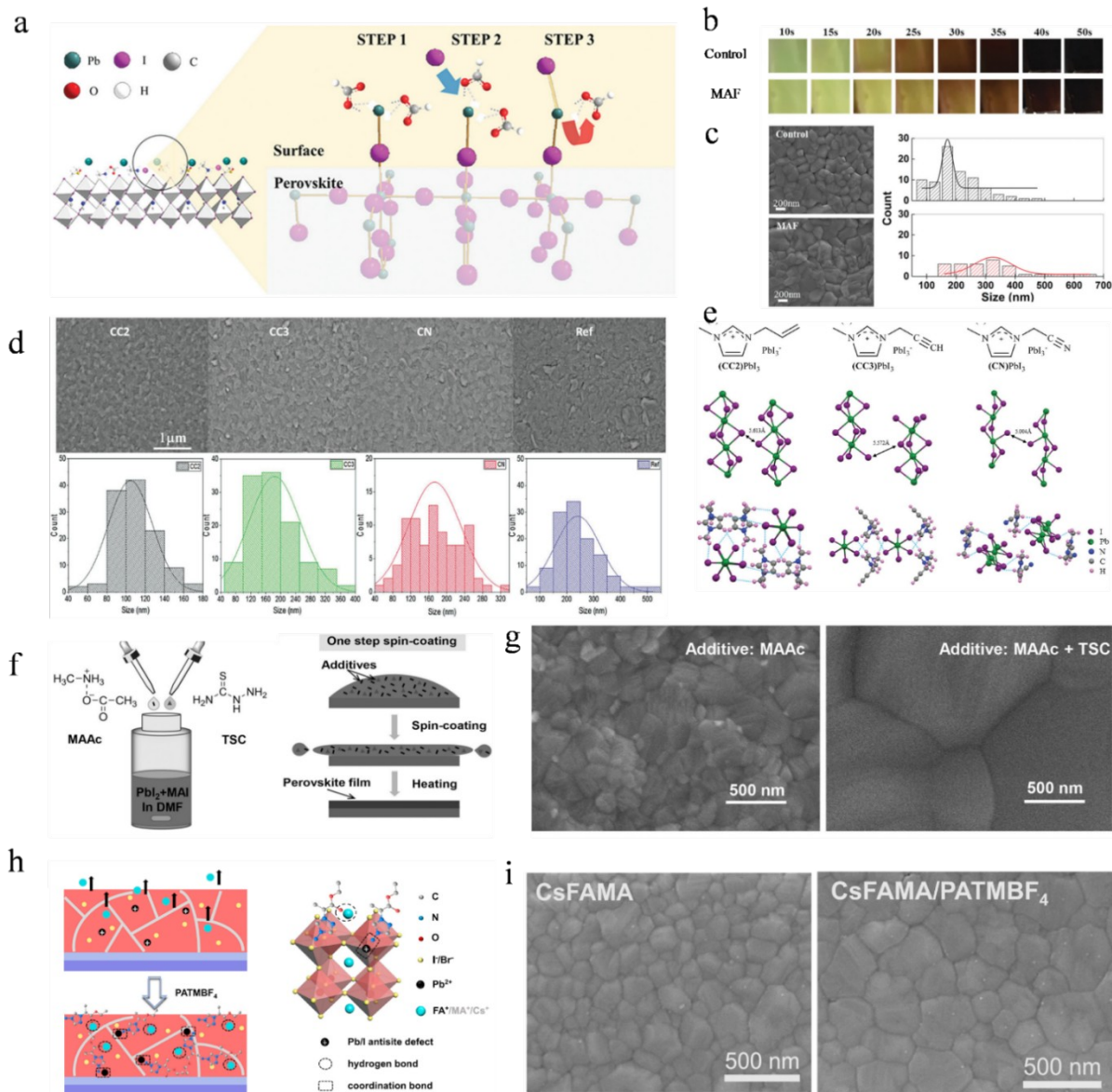
Figure 2. (a) Schematic of the proposed perovskite crystal growth mechanism as controlled by the formate anions. (b) Images of perovskite filmsMA collected in annealing temperature of 100 °C. (c) (left) SEM images of control and MAFa-treated perovskite films and corresponding grain sizes distribution by nano measurer. Copyright 2016 Wiley-VCH.[44] (d) SEM images of perovskite films with CC2, CC3, CN compared to the reference and corresponding grain sizes distribution. (e) Structures of (CC2)PbI₃, (CC3)PbI₃ and (CN)PbI₃. Top:schematic of the salt. Middle: X-ray structures showing the infinite $[PbI_3^-]_n$ chains with the shortest I-I distance indicated. Bottom: hydrogen bonding between the cations and the anions. Copyright 2017 Wiley-VCH.[45] (f) Schematic diagram of MAAc and TSC additive-assisted one-step deposition of perovskite thin films. (g) SEM images of perovskite films with additives of MAAc and MAAc+TSC. Copyright 2017 Wiley-VCH.[46] (h) Schematic diagram

of mechanism of ionic liquid acting on perovskite film. (i) SEM images of the CsFAMA and CsFAMA/PATMBF$_4$ films. Copyright 2021 Elsevier Ltd.[47]

Table 1. Summary of the photovoltaic parameters of PSCs with ILs in perovskite precursor solution engineering.

ILs	Function	Perovskite	Jsc (mA/cm^2)	Voc (V)	FF (%)	PCE (%)	ref
MAFa	As additives	MA$_{0.17}$FA$_{0.83}$Pb(I$_{0.83}$Br$_{0.17}$)$_3$	22.70	1.14	71.00	19.50	[44]
IL with CC$_2$	As additives	MAPbI$_3$	22.62	1.09	78.00	19.21	[45]
HMII	As additives	FAPbI$_3$	24.85	1.07	78.00	20.60	[48]
MAAc	As additives	MAPbI$_3$	23.17	1.12	75.70	19.19	[46]
MAAc	As additives	CsPbBr$_3$	7.19	1.23	73.10	7.37	[49]
1-EC	As additives	MAPbI$_3$	17.34	0.91	75.24	11.80	[50]
HMImCl	As additives	MAPbI$_3$	11.90	0.92	49.00	5.10	[51]
[TBAM][CL]	As additives	MAPbI$_3$	13.50	0.84	51.00	5.63	[52]
FAAc	As additives	FASnI$_3$	23.20	0.59	72.76	9.96	[53]
MA$^+$CF$_3$COO$^-$	As additives	MAPbI$_3$	22.70	1.15	77.10	20.1	[54]
ILPF$_6$	As additives	MAPbI$_3$	21.49	0.97	62.09	13.01	[55]
BMIBr	As additives	FASnI$_3$	19.86	0.70	72.36	10.09	[56]
tTPPI	As additives	MAPbI$_{3-x}$Cl$_x$	19.70	0.90	73.00	13.00	[57]
BMII	As additives	MAPbI$_3$	21.58	1.04	70.00	15.60	[58]
MAAc	As additives	MAPbI$_3$	23.68	1.06	68.00	17.07	[59]
ZIL	As additives	(FAPbI$_3$)$_{1-x}$(MAPbBr$_3$)$_x$	24.85	1.16	78.00	22.52	[60]
BAAc	As additives	BA$_2$MA$_{n-1}$Pb$_n$I$_{3n+1}$	16.75	1.31	74.07	16.52	[61]
EATZ	As additives	MAPbI$_3$	23.39	1.10	77.84	20.03	[62]
MAAc	As additives	MAPbI$_3$	22.69	1.02	82.00	18.91	[30]
6CNBP-N	As additives	MAPbI$_3$	22.35	1.13	81.00	20.45	[25]
HMImCl	As additives	Cs$_{0.05}$(FA$_{0.83}$MA$_{0.17}$)$_{0.95}$Pb(I$_{0.83}$Br$_{0.17}$)$_3$	25.31	1.09	70.00	19.44	[63]
1-EC	As additives	MAPbI$_3$	20.69	0.96	75.80	15.14	[64]
PATMBF$_4$	As additives	Cs$_{0.05}$(FA$_{0.85}$MA$_{0.15}$)$_{0.95}$Pb(I$_{0.85}$Br$_{0.15}$)$_3$	23.74	1.11	81.02	21.35	[47]
MPIB	As additives	MAPbI$_3$	19.83	1.11	82.10	18.22	[23]
MAFa	As solvent	MAPbI$_3$	NA	NA	NA	NA	[65]
MAFa	As solvent	MAPbI$_3$	NA	NA	NA	NA	[28]
MAFa	As solvent	FAPbI$_3$	25.34	1.17	81.36	24.1	[66]
MAAc	As solvent	MAPbI$_{3-x}$Cl$_x$	23.16	1.11	78.01	20.05	[67]
MAAc	As solvent	CsPbI$_{2.5}$Br$_{0.5}$	17.67	1.30	74.18	17.10	[68]
MAAc	As solvent	FA$_x$MA$_{1-x}$PbI$_3$Br$_{3-x}$	24.39	1.17	76.87	22.00	[69]
MAAc	As solvent	MASn$_x$Pb$_{1-x}$I$_3$	25.30	0.85	71.70	15.42	[70]
MAAc	As solvent	(MTEA)$_2$(MA)$_4$Pb$_5$I$_{16}$	21.77	1.09	76.27	18.06	[71]
MAP	As solvent	(MA$_{0.15}$FA$_{0.85}$)Pb(I$_{0.85}$Br$_{0.15}$)$_3$	23.08	1.07	62.00	15.46	[27]
MAP	As solvent	MAPbI$_3$	23.39	1.12	78.48	20.56	[72]

Other ILs containing imidazoloium have also been applied as precursor solution additives. Akin et al.[48] employed 1-hexyl-3-methylimidazolium iodide (HMII) IL to facilitate the grain coarsening based on its high polarity and high boiling point. The additive had an apparent effect on the crystallization, resulting in uniform film morphology with larger domains compared to the reference. From the theoretical perspective, the classic coarsening mechanism of solid-state grain growth has been often used to explain such effects on the crystal growth of perovskites. Addition to IL is thought to contribute to Ostwald ripening and coarsening process during the thermal annealing which ultimately alters and size and morphology of the perovskite grains.[56]

In an alterntive approach, ILs were combined with other additives to improve the quality of the perovskite films. Wu et al.[46] introduced the IL methylammonium acetate (MAAc) and thiosemicarbazide (TSC) in perovskite precursor solutions to alter the morphology and crystal quality. Highly uniform perovskite films with full coverage morphology were prepared with 10–15% MAAc in a stoichiometric precursor solution folowed by one-step spin-coating (Figure 2f). The resulting thin films with MAAc showed full coverage and uniform morphology (Figure 2g). However, the average size of the crystals was <300 nm, which was not favorable for transport and collection of photogenerated charges. Another TSC was used to increase the crystal size and the synergy between the two additives resulted in high-quality films and a 19.58% PCE.

MAAc as an additive was also utilized in all-inorganic $CsPbBr_3$ perovskite.[49] uang et al. proposed a new strategy to introduce cesium acetate (CsAc) and MAAc to increase the concentration of the $CsPbBr_3$ precursor solution, which afforded perovskite films with high coverage. $Cs_xMA_{1-x}PbBr_3$ was first formed after spin coating and low temperature annealing, and it was found that a lot of MAAc and MABr adsorbed onto or wrapped around the $Cs_xMA_{1-x}PbBr_3$ grains. Owing to the coordination between Ac^- and Pb^{2+}, the crystallization of $Cs_xMA_{1-x}PbBr_3$ crystals was delayed, which lead to uniform nucleation sites and high coverage. As the temperature was increased, MA^+ was gradually replaced by Cs^+ to form $CsPbBr_3$. In addition to these ILs, 1-ethylpyridinium chloride (1-EC)[50,64], 1-hexyl-3-methylimidazolium chloride (HMImCl)[51,63], tetrabutylammonium chloride ([TBAM][CL])[52], n-butylammonium acetate (BAAc)[61], formamidine acetate (FAAc)[53] and 1-ethylamine hydrobromide-3-methylimidazolium hexafluorophosphate (ILPF$_6$)[55] have been developed

respectively to attain a control over the crystal growth and for regulation of the film morphology.

The examples provided above are related to one-step preparation technology for perovskite solar cells with ILs as additives in the precursor solution. A two-step method has also been developed to prepare perovskite films which provides full coverage and better solvent selectivity.[73,74] However, challenges remain. In the spin-coating of the PbI_2 layer, the low solubility of PbI_2 affects the quality of the perovskite film.[75] In the spin-coating step of the organic layer, the diffusion of the layer is affected by rapid nucleation of the perovskite at the interface which results in low transformation of PbI_2.[76,77] To solve these issues, in the two-step method Chen et al.[58] added 1-butyl-3-methylimidazolium iodide (BMII) directly into the PbI_2 solution. The BMII significantly enhanced the solubility of PbI_2, presumably by disruption of van der Waals interactions between the layered PbI_2 crystals, and led to high coverage and uniform PbI_2 film. Importantly, the coordination between PbI_2 with BMII occured before the reaction between MAI and PbI_2, which effectively improved the kinetics of the interfacial reaction, resulting in better control of the perovskite formation. The corresponding perovskite film test result of SEM, XRD and TRPL illustrate that 1% BMII enhanced perovskite crystallization, resulting in large grains, strong absorption and fewer defects. The additive MAAc was also introduced in PbI_2 solution by Xiao et al.[59] to improve the quality of the film and enhance the performance through the two-step spin-coating process. The difference in color between the PbI_2/MAPbI$_{3-x}$(Ac)$_x$ film from the first spin-coating step and the PbI_2 layer indicated chemical change. The MAPbI$_{3-x}$(Ac)$_x$ thus obtained acted as seed to generate a high quality film in the second spin-coating step. The high quality of the film with large grains and uniform were reflected in a PCE of 17.07%, which is superior to the control device that did not contain MAAc.

ILs were also dissolved in organic salts as additives and spin-coated on PbI_2 films to obtain high-quality perovskite films. Yang et al.[60] iincorporated a zwitterionic ionic liquid (ZIL) into organic salts to prepare high-quality films, and the corresponding ZIL-treated PSCs had a PCE of 22.5% with an outstanding long-term stability. The chemical interactions between BF_4^-, zwitterions and perovskite components are thought to play an important role in generating better crystallinity and grain boundary passivation defects. However, the addition of IL additives into organic salts also brings difficulties with diffusion of IL and more

involved synthetic protocols. Selecting IL additives with the appropriate solubility and viscosity for perovskite film via the two-step preparation approach remains a major challenge to be addressed in a future research. Therefore, the current research is less and a lot of researchs are being explored.

2.3. Ionic liquids as a sole solvent in perovskite precursor solutions

Most of the currently used solvents for preparation of perovskite devices are either not environmentally friendly or outright toxic, with DMSO, DMF, DMAc and NMP being most commonly used.[78,79] Water, ethanol and acetonitrile (ACN) have been considered as possible substitutes in perovskite precursor solution. However, the performance of solar cells based on these solvents has been found to be inferior compared the common organic solvents, and the preparation process is more complex.[11] Therefore, a suitable alternative material or approach was sought for as a green and non-toxic medium for preparation of the perovskites.

ILs are known for their ability to completely dissolve various perovskite precursor solutions by establishing strong chemical interactions between the solute and the solvent.[80] Meanwhile, Ils as the sole solvent can induce directional crystallization and promote the transformation of the precursor solution to perovskite crystals by forming active intermediates.[69] As early as in 2015, Moore et al.[65] found that traditional organic solvents can be replaced by the IL methylammonium formate (MAFa) to dissolve a mixture of PbI_2 and MAI to prepare perovskite films. This was a fundamentally new strategy that allowed for the ILs to be used as a sole solvent in the perovskite precursor solution. Similarly, Hui et al.[66] employed the IL MAFa as an alternative solvent for DMF and DMSO to prepare a black-phase $FAPbI_3$ perovskite in the air. The corresponding device displayed a power-conversion efficiency of 24.1% and retained 93% of its original PCE within 5000 hours in nitrogen. Taking advantage of the strong C=O···Pb chelation and hydrogen bonds N–H···I in MAFa with PbI_2 (Figure 3a), PbI_2 grows vertically on the substrate (Figure 3b). This provides a convenience with formamidinium iodide (FAI) entering the PbI_2 films, and results in decrease of the formation energy barriers (Figure 3c). The obtained $FAPbI_3$ films with MAFa as single solvent for the perovskite precursor solution had large grain size and long carrier lifetime due to high crystal quality and low defect density.

11
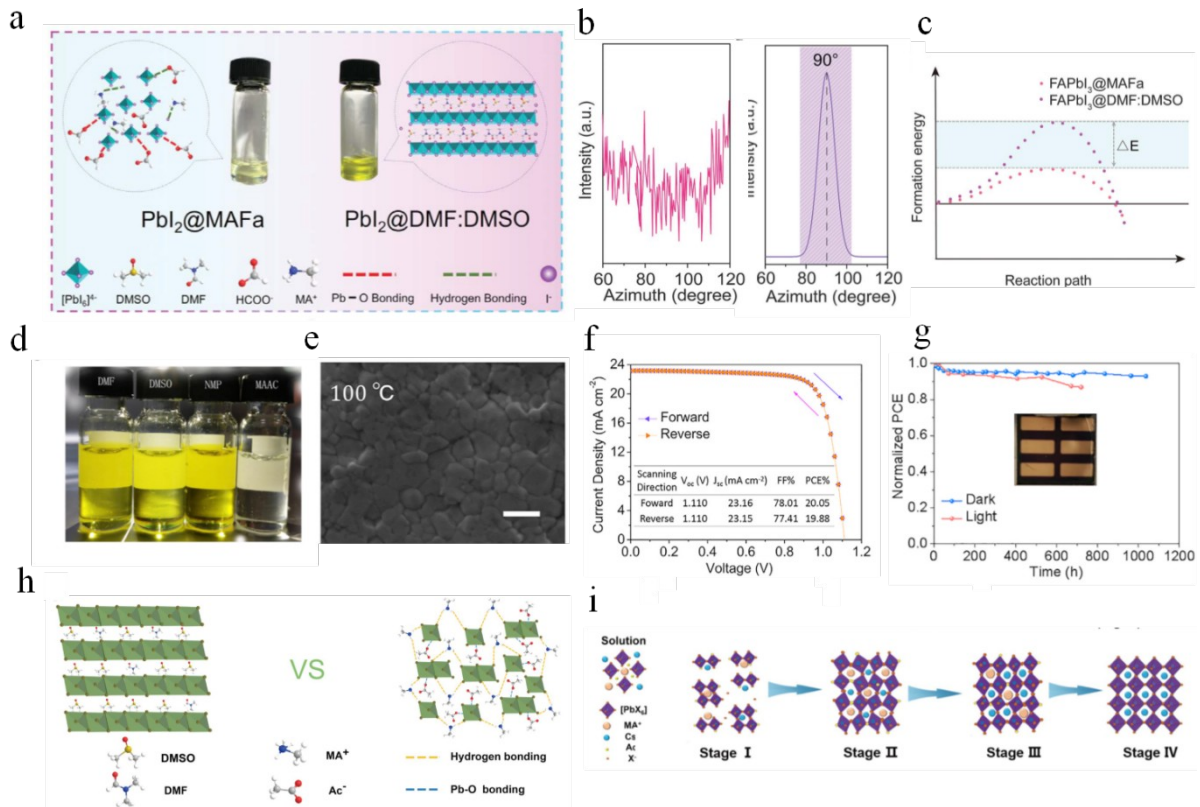
Figure 3. (a) Schematic diagram of interactions in the PbI₂@MAFa and PbI₂@DMF:DMSO solutions. (b) Azimuth integration at q ≈ 9.25 nm⁻¹ for PbI₂@DMF:DMSO and PbI₂@MAFa thin films from in situ GIWAXS spectra. (c) Schematic diagram of perovskite crystallization kinetics of FAPbI₃ film under PbI₂@MAFa (pink) and PbI₂@DMF:DMSO (purple) films, respectively. Copyright 2021 American Association for the Advancement of Science.[66] (d) An image of perovskite precursor solution of solvents DMF, DMSO, NMP and MAAc. (e) SEM images of perovskite films fabricated under the temperature of 100 ℃, the scale bar represents 500 nm. (f) J-V curves of MAAc-PSCs. (g) Stability of MAAc-PSCs without encapsulation under dark and light conditions. Copyright 2019 Elsevier Inc.[67] (h) Interaction in the precursor solutions using DMFO, DMF and MAAc as solvent. (i) Schematic diagram of CsPbI₂Br crystallization process. Copyright 2020 Wiley-VCH.[68]

The IL methylammonium acetate (MAAc) was also often used as a single solvent in perovskite precursor solutions due to its solubility in inorganic and organic salts. Very recently, Gu and colleagues systematically revealed the formation mechanism of stable perovskite precursor solutions through employing MAAc as solvent.[81] Specifically, The existent of coordination interaction between O=C-O⁻ and Pb²⁺, N–H•••O=C-O⁻ hydrogen bonds and van der Waals force in MAAc system promote the formation of regular-orientated gel-

like colloids lamellae in perovskite precursor solutions. Therefore these stable colloids in perovskite precursor solutions using the MAAc as solvent exhibit excellent stability under air aging, heat stress and electrolytic dissociation conditions, which provides a basis for obtaining high-quality and stable perovskite films. Chao et al.[67] demonstrated that both methylammonium and lead salts can be completely dissolved in MAAc because of the formation of hydrogen bonds in solution (Figure 3d). Thin films based on MAAc as solvent are dense, and their preparation is reproducible and circumvents the complexities of the anti-solvent process. It was observed that a higher total colloid concentration at the same concentration of perovskite precursor solution owing to the weak interaction between MAAc with the perovskite precursor PbI_2 and methylamine hydrochloride (MACl), compared to DMF/DMSO solution, which affected the growth ability and uniformity of the crystals (Figure 3e). After optimization, the devices had a maximum efficiency of 20.05% (Figure 3f) and maintained > 93% of their initial efficiency in air (Figure 3g). In IL MAAc system of perovskite precursor solution, Firstly, the dissolution of PbI_2 and MAI in MAAc to form a weak electrolyte $Pb(Ac)_2$ through the combine of CH_3COO^- (Ac^-) and Pb^{2+}. Subsequently, the emergence of evaporating CH_3COOH (HAc) and CH_3NH_2 (MA) as the heating process due to thermodynamic instability of $Pb(Ac)_2$ was discovered to promote the formation of $CH_3NH_3PbI_3$. Notably, the mechanism of crystallization regulation through the introduction of IL MAAc inhibit the the formation of multiple intermediate phases, which reduce the pathways of generating defects.[69]

MAAc was also employed as single solvent in perovskite precursor solution for manufacturing all-inorganic perovskite solar cells. Wang et al.[68] reported a new tailoring strategy to manufacture all-inorganic $CsPbI_{3-x}Br_x$ perovskites through strong interaction between C=O with lead (Pb^{2+}) and N-H$\cdots$I hydrogen bond introduced by the IL MAAc as solvent (Figure 3h). These interactions stabilize the perovskite precursor solution and form high-quality films by delaying the crystallization. In a subsequent spin-coating and annealing process, the MAAc $CsPbI_2Br$ film formation occured in four steps, as confirmed by X-ray diffraction (Figure 3i). In the first step, an intermediate phase $Cs_{1-x}MA_xPbAc_xI_{2-x}Br$ appeared before the annealing, when a large amount of MAAc exist in the perovskite crystal lattice owing to the insufficient temperature for its evaporation. The existence of intermediate phase leads to delayed crystallization of the $CsPbI_2Br$ crystal films.[49] In the second step, MAAc was slowly evaporated as the annealing temperature increased, and resulted in the formation

of the intermediate phase $CsPbI_yBr_{3-y}$ by incorporation of CsI and PbI_2 into the lattice. In the third step, MAAc continued to evaporate at 120–150 °C, and both intermediates $Cs_{1-x}MA_xPbAc_xI_{2-x}Br$ and $CsPbI_yBr_{3-y}$ gradually disappeared, which stabilized the crystals. Finally, in the fourth step, at higher annealing temperature of 150 °C the intermediate phases disappeared completely, and no MAAc residue remained (Figure 3j). The optimized device based on the above process showed a PCE of 17.10% with long service life over 1500 h under continuous light illumination. Recently, MAAc IL have been developed as a sole solvent to fabricate Sn-Pb based PSCs with antisolvent-free processing by Chen and co-workers.[70] With the assistance of multiple organic halides on the crystallization process of Sn-Pb perovskite, the high-quality Sn-Pb film with large grain size and smooth surface and Sn-Pb based PSCs with a champion PCE of 15.42% was obtained through the solvent engineering of MAAc IL.

Considerable attentions were also focused on ILs as solvents or spacer in perovskite precursor solution engineering for the preparation of 2D perovskite devices. Chen and co-workers employed the IL n-butylamine acetate (BAAc) as spacer to replace the traditional halide spacer n-butylamine iodide to endow the 2D PSCs with the champion PCE of 16.25%.[61] In BAAc system, the formed strong chelation and hydrogen bonding between IL BAAc and the perovskite framework promoted the formation of phase-pure quantum well (QW) films, which is beneficial to the enhancement of carrier transport and stability. In addition, these interactions in perovskite precursor solution of BAAc system suppress the aggregation of colloids, leading to the formed particles with a narrow size distribution of 0.6 nm. Based on these advantages, the obtained phase-pure QW films exhibited a smooth surface with a large grain size. Another research about two-dimensional Ruddlesden–Popper phase (2DRP) PSCs was reported by Chen and colleagues that the application of MAAc as solvent and alkylammonium 2-(methylthio) ethylamine hydrochloride (MTEACl) as the bulky ammonium into formation of $(MTEA)_2(MA)_4Pb_5I_{16}$ perovskite.[71] Besides the traditional van der Waals interactions, the existent of S-S interaction in the 2DRP perovskites $(MTEA)_2(MA)_4Pb_5I_{16}$ through the involvement of MTEACl promoted the improved crystallinity and oriented growth. Consequently, the corresponding 2D PSCs achieved the certified PCE of 17.8% and excellent stability up to 1,512 h under R.H 70% humidity conditions.

3. Charge transport layer engineering with ionic liquids

3.1. Effect of ionic liquids on charge transport

One of the endeavors in perovskite devices is focusing on charge transport, charge carrier extraction and growth in the transport layer, which are germane to achieving high PCE and stability.[82,83] This aspects is related to challenges with optimization of the charge transport layer materials owing to the poor charge mobility in the traditional transport layer materials. [84] ILs were used not only in perovskite precursor solutions, but also in transport layer materials to effectively improve their transport capacity. According to the effect of the charge transport layer, the function of ILs as doping materials in the electron transport layer (ETL), the hole transport layer (HTL) and the single electron transport layer (ETL) are discussed separately below. Table 2 summarizes the recent progress of ILs in charge transport layer engineering.

Table 2. Summary of the photovoltaic parameters of PSCs with ILs in charge transport layer engineering.

ILs	Function	Transport layer material/ Perovskite	Jsc (mA/cm^2)	Voc (V)	FF (%)	PCE (%)	ref
TMAH	As ETL dopant	TMAH-SnO$_2$/FA$_{0.75}$MA$_{0.25}$PbI$_{2.5}$Br$_{0.5}$	23.31	1.14	77.37	20.52	[85]
BenMeIM-Cl	As ETL dopant	C$_{60}$/CH$_3$NH$_3$PbBr$_3$	6.14	1.39	69.94	5.88	[86]
BenMeIM-Cl	As single ETL	IL/(FAPbI$_3$)$_{0.85}$(MAPbBr$_3$)$_{0.15}$	22.72	1.07	66.20	16.09	[87]
BIPH-II	As single ETL	IL/MAPbI$_3$	22.40	1.08	71.40	17.31	[88]
[EMIM]PF$_6$	As single ETL	IL/CH$_3$NH$_3$PbI$_3$	21.04	1.04	59.43	13.23	[89]
MAAc	ETL-Free	IL/MAPbI$_3$	22.40	1.15	81.60	21.08	[90]
BMPyTFSI	As HTL dopant	Spiro-OMeTAD/ (FAPbI$_3$)$_{0.85}$(MAPbBr$_3$)$_{0.1}$	21.37	0.95	73.45	14.96	[15]
PVBI-TFSI	As HTL dopant	Spiro-OMeTAD/ K$_{0.05}$(MA$_{0.15}$FA$_{0.85}$)$_{0.95}$PbI$_{2.55}$Br$_{0.45}$	22.99	1.16	76.00	20.33	[91]
BuPyIm-TFSI	As HTL dopant	Spiro-OMeTAD/ CH$_3$NH$_3$PbI$_3$	16.26	0.87	56.00	7.91	[92]
BMPyTFSI	As HTL dopant	FDT/Cs$_{0.1}$(FAPbI$_3$)$_{0.81}$(MAPbBr$_3$)$_{0.09}$	22.95	1.07	74.00	18.24	[93]
EMIC	As HTL dopant	PEDOT:PSS/CH$_3$NH$_3$PbI$_3$	23.91	1.08	78.00	20.06	[94]
[C12mim]Br	As HTL dopant	P3CT-K/MAPbI$_3$	22.22	1.05	80.79	18.81	[95]
BuPyIm-TFSI	As HTL dopant	X60/(FAPbI$_3$)$_{0.85}$ (MAPbBr$_3$)$_{0.15}$	22.49	1.04	69.00	14.65	[96]

3.2. Electron transport layer (ETL) dopant

The ETL is usually located between the cathode and the perovskite layer to extract photo-generated electrons and transport them to the external circuit.[97] The performance of the ETL plays a crucial role on photocurrent density (J_{SC}), open-circuit voltage (V_{OC}), and fill factor (FF) of the device performance.[98,99] TiO$_2$, ZnO, SnO$_2$ and C$_{60}$ have been used as an ETL material for high-efficiency PSCs. Among them, SnO$_2$ has attracted attention, and is regarded as an ideal ETL material because of its excellent chemical stability and high electron mobility.[100] However the capacity of SnO$_2$ as a growth platform for high-quality perovskites and charge extraction necessitate further improvement to meet the requirements for practical applications. Huang et al.[85] employed the IL tetramethylammonium hydroxide (TMAH) as additive for SnO$_2$ nanocrystals to significantly enhance the conductivity of the SnO$_2$ for efficient electron extraction and charge transport at the perovskite grain boundaries. After adding an IL to SnO$_2$, the interplanar spacing of the SnO$_2$ particles was 0.333 nm (Figure 4a), an indication of the excellent crystallinity of TMAH-SnO$_2$ nanoparticles. Furthermore, the conduction band edge recorded from the ultraviolet photoelectron spectrometry (UPS) results, was also affected by this modification (Figure 4b). Apparently, the LUMO of the perovskite was level with the conduction band edge of n-SnO$_2$. A different situation is encountered with the conduction band edge of TMAH-SnO$_2$, which is 0.16 eV higher than the LUMO of the perovskite to restrain the interface recombination, and leads to higher efficiency (Figure 4c). Based on TMAH-SnO$_2$ ETL layer, perovskite thin films without any observable pinhole were obtained (Figure 4d). The respective devices displayed efficiency of 20.28%, with the short-circuit current density (Jsc), fill factor (FF) and open-circuit voltage (Voc) being 22.51 mA cm^{-2}, 79% and 1.141 eV, respectively.

Fullerene (C$_{60}$) and its derivatives were also employed as ETL materials for efficient PSCs, and they are currently placed between the electrode and the perovskite layer to form a p–i–n structure.[101] However, the obvious shortcoming of fullerene appears to be the poor ability to form films, ordinary electron conductivity and poor wettability, which hinders the further development of PSCs.[102] Luan et al.[86] provided an alternative solution by using ionic liquids, 1-benzyl-3-methylimidazolium chloride, which was incorporated into C$_{60}$ in a planar n-i-p structure CH$_3$NH$_3$PbBr$_3$ solar cells to effectively decrease the work function and enhance the wettability of the perovskite layer on C$_{60}$. The work function (WF) schematic of FTO/four ETLs/perovskite/SpiroO-MeTAD/Au is estimated in Figure 4e, and the results illustrated the function of IL for decreasing the interface barrier between the perovskite layer and the

cathode. Movever, the addition of IL also had an impact on the light absorption when mixed with C_{60}, which effectively improved the problem of partial dissolution of C_{60} (Figure 4f). As a result, the PCE of the device fabricated on IL/C_{60} was 5.88%, compared to the devices of 1.59%, 2.24% and 2.41% based on FTO/IL, FTO/C_{60} and FTO/C_{60}/IL.
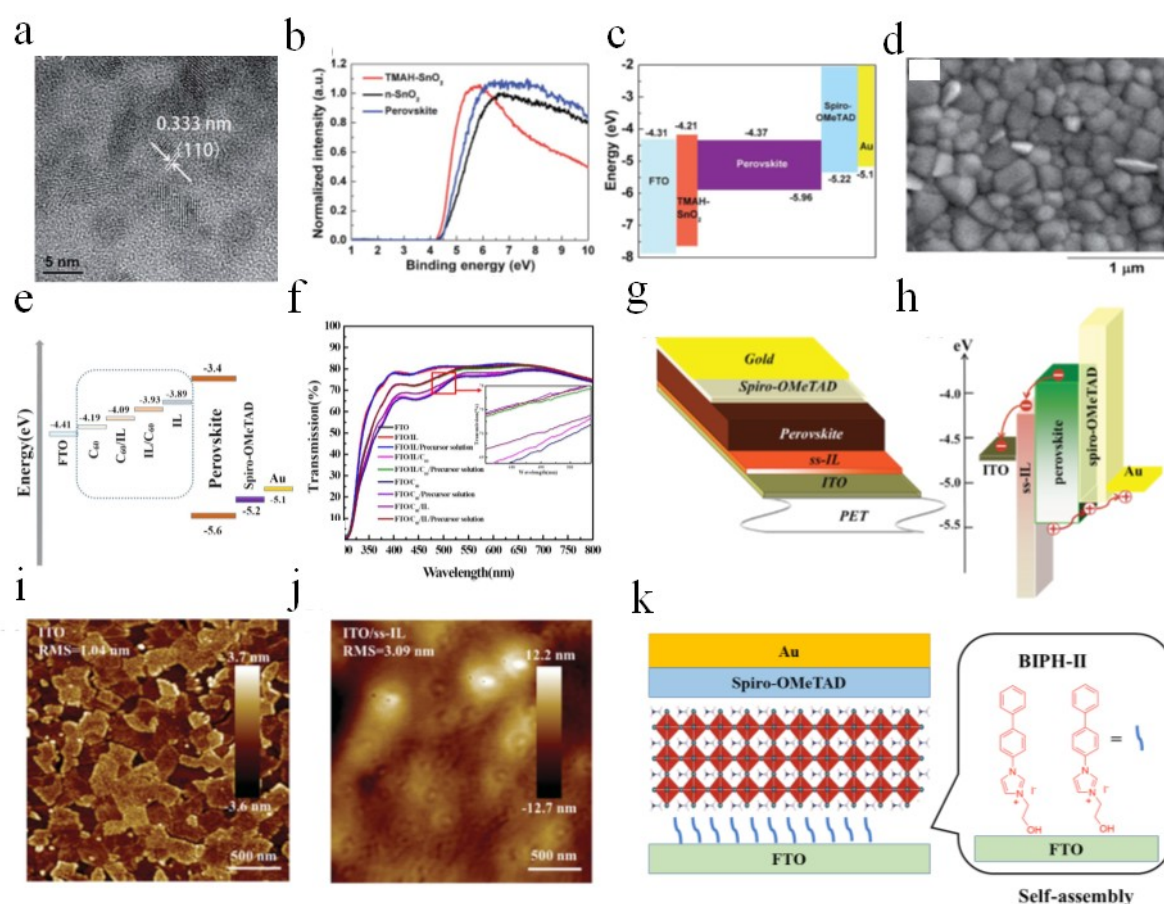

Figure 4. (a) TEM image of TMAH-modified SnO_2 nanoparticles. (b) Ultraviolet photoelectron spectroscopy (UPS) cut-off edge of n-SnO_2, TMAH-SnO_2, and the perovskite. (c) Schematic illustration of the band alignment of TMAH-SnO_2 and the perovskite, according to the UPS data. (d) Surface SEM image of the perovskite layer on 1.0% TMAH-SnO_2. Copyright 2018 The Royal Society of Chemistry.[85] (e) Energy diagram of devices based on IL, C_{60}, C_{60}/IL and IL/C_{60} as ETLs. (f) Transmission spectra of four different ETL layer and the corresponding ETL layer treated by perovskite precursor solvent. Copyright 2019 Elsevier Inc.[86] (g) The structure of the PSCs with ss-IL as the ETL layer. (h) Energy-level diagram of the PSCs. (i,j) AFM height images of ITO and ITO/ss-IL samples. Copyright 2020 Wiley-VCH.[87] (k) The device structure of the perovskite solar cell with BIPHII as ETL. Copyright 2020 Wiley-VCH.[88]

3.3. Single electron transport layer (ETL) and ETL-free structure

The ETL that are currently used require harsh and complex processing and preparation conditions, and also have poor film-forming ability. Finding alternatives to these traditional ETL materials for industrialization in order to simplify the process and reduce the preparation cost has been one of the main goals of research.[103] Due to the excellent stability and ionic conductivity, ILs are considered to hold potential as single ETL layer. Yang et al.[87] developed the efficient flexible PSCs with low-temperature processing by application of 1-benzyl-3-methylimidazolium chloride (ss-IL) as the single ETL layer (Figure 4g). Taking advantage of high electron mobility and suitable work function for matching perovskite (Figure 4h), ss-IL was proven to be able to reduce the electron trap-state density and eliminate hysteresis. Furthermore, the uniform coverage of the ETL film formed by ss-IL provided a good foundation for growth of perovskite and favorable interface contact relative to the bare ITO substrate (Figure 4i,j). The flexible devices modified with ss-IL exhibited an increased PCE of 16.09%. Another IL, hydroxyethyl functionalized imidazolium iodide (BIPH-II), was reported by Cheng et al.[88] to serve as independent ETL layer for a remarkable enhancement of the PCE of PSCs at 17.31% (Figure 4k). The strong interaction between the hydroxylethyl group in BIPH-II IL with the FTO substrate affected the work function (WF) of FTO, resulting to more matching energy levels. The WF of the FTO decreased from 4.60 eV to 4.40 eV after the modification of the IL, and the upward work function is beneficial to realize excellent photoelectric performance. Moreover, the electron extraction and interfacial charge recombination were also significantly improved. In a related work, Wu et al.[89] utilized the IL 1-ethyl-3-methylimidazolium hexafluorophosphate ([EMIM]PF_6) as an independent ETL in PSCs. The devices displayed a record PCE of 14.39% that is close to the corresponding devices using TiO_2 as ETL layer. These results indicated that [EMIM]PF_6/IL possessed a capability of charge transfer which is similar to TiO_2, however it is more processible at low temperatures and this simplifies the preparation process. [EMIM]PF_6/IL can also be appiled to modify the TiO_2 layer in order to obtain better devices. [EMIM]PF_6/IL as a modifier on TiO_2 showed a significant effect on defect passivation, ion migration and electron mobility. Consequently, the highest PCE based on [EMIM]PF_6-IL modified TiO_2 ETL was 19.59%, showing an improvement compared to the TiO_2 ETL-based PSCs (~29.8%). In general, IL as a single ETL layer simplified the preparation process and is suitable for commercial low-

temperature production, but the development of new ILs needs to be continued for optimizing the devices to high efficiency. Especially as the ETL materials, more research efforts need to be made on ILs as a separate ETL material with better device performance. Considering the current practicability and maturity, ILs as ETL dopant appear to be more effective in terms of efficiency right now.

In addition to the application of IL for a single ETL layer in PSCs, ILs have been also employed to fabricate ETL-free PSCs. Huang and colleagues proposed a new charge transport layer engineering strategy of obtaining the ETL-free PSCs through the introduction of MAAc ILs into perovskite precursor solution as a pure solvent.[90] MAAc IL can act as the role of modifier at ITO/perovskite interface to match the electronic energy band configuration for effective carrier separation and collection due to the formation of an interfacial dipole layer through the physical adsorption of the MAAc molecules on the ITO electrode. Taking the advantage of in-situ dipole layer, the PSCs with ETL-free structure achieved the champion PCE of 21.08%. Notably, this promising strategy of employing the ILs to fabricate ETL-free PSCs has significantly simplified the manufacturing process with the low cost.

3.3. Hole transport layer (HTL)

The history of optimization of PSCs has witnessed the significance of reducing charge-recombination loss and improving charge mobility at the carrier transport layers.[104] Analogous to the relevance of the ETL in the perovskite solar cells, HTL plays an important role for efficient hole extraction and avoidance of charge recombination processes, contributing to the high performance of the PSCs.[105] Spiro-OMeTAD, as the most commonly used HTL material with lithium bis(trifluoromethanesulfonyl)imide (LiTFSI), and 4-tert-butylpyridine (t-BP) as additive have been researched for efficient PSCs.[106] However, the hysteresis and stability of PSCs was affected by both t-BP and LiTFSI, limiting the commercial production and application of the perovskite. Hence, Calio et al.[15] applied the IL 1-butyl-3-methylpyridinium bis(trifluoromethylsulfonyl)imide (BMPyTFSI) as dopant into HTL Spiro-OMeTAD to enhance the conductivity and lifetime of the corresponding PSCs through hydrophobicity of the ILs (Figure 5a). The presence of a peak at 520 nm in the UV-vis spectrum reveals the function of BMPyTFSI as a p-type dopant that oxidizes spiro-

OMeTAD (Figure 5b). In the oxidation process, a weak bond is formed between the anion of BMPyTFSI with spiro-OMeTAD$^+$, resulting in p-type doping (Figure 5c).

Geffroy et al.[91] reported poly(1-butyl-3-vinylimidazolium bis(trifluoromethylsulfonyl)imide) (PVBI-TFSI) as p-type dopant of HTL material to enhance conductivity and obtain PSCs without hysteresis and with >20% efficiency. Similarly to earlier research, Zhang et al.[92] initially used the IL N-butyl-N_0-(4-pyridylheptyl)imidazolium bis(trifluoromethane)sulfonimide (BuPyIm-TFSI) as additive to improve the electrical property of HTL and reduce nonradiative recombination of PSCs (Figure 5d). The function of BuPyIm-TFSI was to release free protons to promote the oxidization of spiro-MeOTAD, leading to high concentration and excellent electrical conductivity of HTL. (2′,7′-bis(bis(4-methoxyphenyl)amino) (FDT) was considered as an alternative HTL material to spiro-MeOTAD because of the simple synthesis process and efficient hole transport, which resulted in efficiency of FDT-based devices of over 20.2%.[107] Hydrophobic IL BMPyTFSI as dopant for FDT was employed in the perovskite solar cell system by Ahmad et al.[93] to improve the stability of the underlying perovskite layer and charge transport (Figure 5e). As a result, IL-doped FDT with LiTFSI, t-BP and FK209 as HTL-layer-based devices realized a PCE of 18.24% and individual IL-doped FDT devices is 15.26%, which was significantly superior to pristine FDT-based devices at 3.025%.
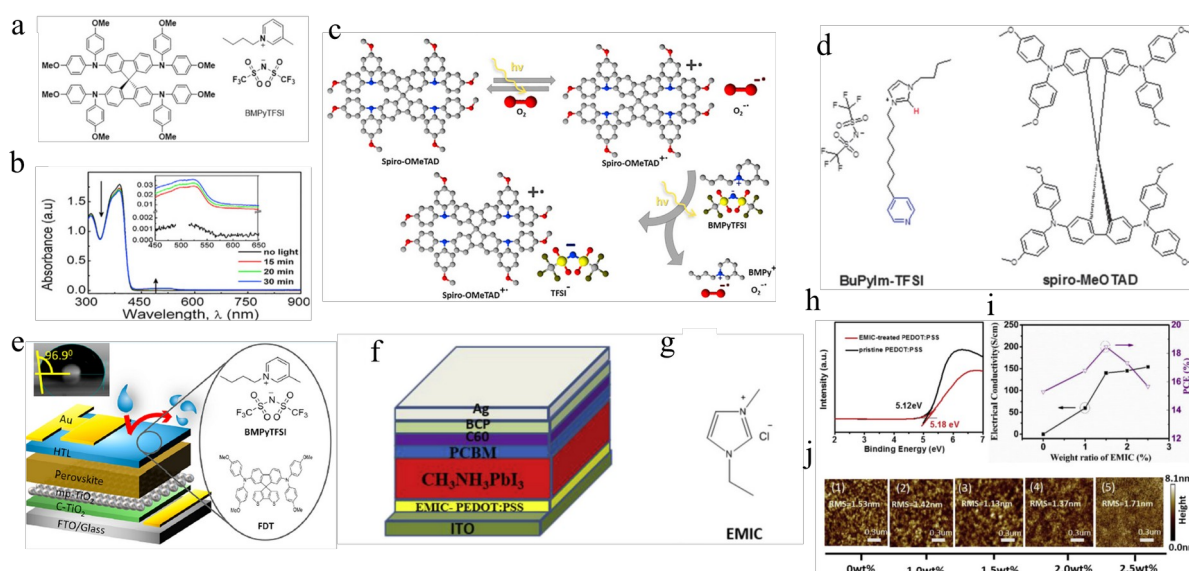
Figure 5. (a) Chemical structures of Spiro-OMeTAD and 1-butyl-3-methylpyridinium bis(trifluoromethylsulfonyl)imide (BMPyTFSI) IL. (b) UV-vis absorption spectra of Spiro-OMeTAD with 7.8 mol% BMPyTFSI. The inset shows the enlarged spectra of the oxidized

Spiro-OMeTAD peak at around 520 nm. (c) Schematic diagram of the oxidation process in Spiro-OMeTAD. Copyright 2018 Elsevier Inc.[15] (d) Chemical structures of the BuPyIm-TFSI and spiro-OMeTAD. Copyright 2018 The Royal Society of Chemistry.[92] (e) Structure diagram of FDT-based device. Copyright 2020 American Chemical Society.[93] (f) Structure diagram of PSC device based on EMIC-PEDOT:PSS as HTL layer. (g) Chemical structure of IL EMIC. (h) UPS spectra of pristine and EMIC-treated PEDOT:PSS films. (i) Electrical conductivities of PEDOT:PSS HTL and PCEs of PSCs based on the different doping concentrations of EMIC in the PEDOT:PSS layer. (j) AFM images of the PEDOT:PSS film with different doping concentrations of EMIC. Copyright 2019 Elsevier Inc.[94]

For the increasingly popular inverted PSCs, PEDOT:PSS has been widely investigated as a hole transport layer material for efficient devices.[108] However, an obvious weakness is the inferior conductivity of PEDOT:PSS that generates excessive loss of energy during the charge carrier transport and weakens the photoelectric performance and stability of the device.[109] To overcome these shortcomings, Zhou et al.[94] utilized the IL 1-ethyl-3-methylimidazolium chloride (EMIC) as dopant in PEDOT:PSS to decrease the work function of the HTL and to enhance electrical conductivity for a high-quality HTL layer (Figure 5f,g). EMIC-doped PEDOT:PSS revealed deeper work function of 5.18 eV compared to the pristine work function of 5.12 eV (Figure 5h), which was beneficial to the reduction of energy barrier between the perovskite layer and HTL as well as to reduction improvement of Voc in PSCs. Furthermore, the smoother surface of PEDOT:PSS with EMIC doping concentrations of 1.5% was obtained, leading to higher FF and J_{SC} owing to a better contact between the perovskite layer and the HTL layer (Figure 5j). The results from electrochemical impedance spectroscopy also showed that the inner series resistance (Rs) and electrical properties were modifed by the EMIC doping, thereby contributing to the high electrical conductivity, low work function and smooth surface to promote the efficient extraction of holes (Figure 5h,j).

Taking the advantage of their excellent solubility and simple processing, conjugated polyelectrolytes (CPEs) have also been considered as a potential HTL material and have been widely researched for high-performance PSCs.[105,110] Nevertheless, the aggregation of CPEs impacts the film morphology and reduces hole mobility.[111] Jian et al.[95] introduced the IL 1-dodecyl-3-methylimidazolium bromide ([C12mim]Br) into potassium poly[3-(4-

carboxylatebutyl)thiophene (P3CT-K) to explore the effect of ILs on the aggregation state of P3CT-K and photoelectric performance of the corresponding devices. [C12mim]Br was inserted into the polymer chain to weaken the interactions between the polymer chains in P3CT-K because of the π–π interactions between imidazole group in the ILs with thiophene backbone of P3CT-K to reduce the aggregation. This decreased aggregation can promote the formation of uniform and smooth HTL films, which further improves the contact between the perovskite layer with the HTL layer for efficient hole extraction. Consequently, the photovoltaic performance on cells based on P3CT-K with a PCE of 16.21% was boosted to 18.81% for [C12mim]Br treated-P3CT-K.

4. Interfacial engineering with ionic liquids

4.1. Challenges with interfaces

The efficiency, stability and preparation process of PSCs need all to be considered to bring these materials closer to the stage where they will be considered for industrial manufacture for practical application.[74,112] The key performance indices are not only affected by the perovskite and transport layers, but also by the interface between the perovskite layer and charge transport layer.[71] In addition to the internal defects of perovskite films, the perovskite films prepared by using traditional methods usually contain defects on their surface, leading to obvious interfacial recombination that limits the *V*oc and FF of the device.[113,114] The interface engineering is an effective strategy to overcome some of these difficulties and to ultimately optimize the performance of the devices. ILs as interfacial modifiers have been widely used for adjusting the work function and remedying defects in interface engineering.[22] Table 3 summarizes the recent progress of the PSCs performance with ILs as interface modifier for regulating the work function and passivating the surface.

Table 3. Summary of the photovoltaic parameters of PSCs with ILs in interfacial engineering

ILs	Function	Device structure	Jsc (mA/cm^2)	Voc (V)	FF (%)	PCE (%)	ref
ImI	Interface Passivation	FTO/ c-TiO2/m-TiO2/ MAPbI$_3$/ ImI/Spiro-OMeTAD/Au	22.02	1.11	81.30	19.90	[115]
[BMMIm]Cl	Interface Passivation	FTO/c-TiO$_2$/m-TiO$_2$/CsPbBr$_3$ /[BMMIm]Cl/Spiro-OMeTAD/Au	7.45	1.61	83.00	9.92	[26]
MATS	Interface	ITO/ PEDOT:PSS/MAPbI3/	24.07	0.94	77.00	17.51	[116]

22

IL	Type	Device Structure	J_{sc}	V_{oc}	FF	PCE	Ref
DMIMPF$_6$	Passivation Interface	MATS/PCBM/Al FTO/TiO$_2$/Cs$_{0.08}$FA$_{0.92}$PbI$_3$/ DMIMPF$_6$/spiro-OMeTAD/Au	25.86	1.11	81.00	23.25	[31]
[BMIM]BF$_4$	Passivation Interface	FTO/NiOx/CH$_3$NH$_3$PbI$_3$/PCBM/ [BMIM]BF$_4$/Ag	23.52	1.06	77.58	19.30	[103]
(PeIm)[TFSI]	Passivation Interface	ITO/ PTAA/ (Cs$_{0.05}$(MA$_{0.17}$FA$_{0.83}$)$_{0.95}$) Pb(I$_{0.83}$Br$_{0.17}$)$_3$ /C$_{60}$/BCP /Cu	22.58	1.17	81.00	21.40	[24]
EMImBF$_4$	Passivation Interface	FTO/NiO/ CH$_3$NH$_3$PbI$_3$/ EMImBF$_4$/ PCBM/BCP	23.40	1.04	78.00	19.00	[117]
[EMIM]Br	Passivation Interface	FTO/SnO$_2$/FAPbI$_3$/IL/Spiro- OMeTAD/Au	25.30	1.19	80.67	24.33	[118]
F-PEAI	Passivation Interface	ITO/PTAA/PEAI/ Cs$_{0.05}$(FA$_{5/6}$MA$_{1/6}$)$_{0.95}$Pb(I$_{0.85}$Br$_{0.15}$)$_3$/ PEAI/PCBM/BCP/Ag	24.13	1.18	84.60	23.72	[119]
[BMIM]BF$_4$	Work Function Optimization	FTO/m-TiO$_2$/ CH$_3$NH$_3$PbI$_3$/ PTAA/Au	22.75	1.12	77.00	19.62	[120]
[BMIM]BF$_4$	Work Function Optimization	FTO/TiO$_2$/[BMIM]BF4/ CH$_3$NH$_3$PbBr$_3$/Spiro-OMeTAD/Au	7.07	1.38	61.29	5.98	[39]
[BMIM]BF$_4$	Work Function Optimization	FTO/SnO$_2$/BMIMBF$_4$/ FA$_{0.83}$MA$_{0.17}$Pb(I$_{0.83}$Br$_{0.17}$)$_3$ /Spiro- OMeTAD/Au	22.70	1.16	79.00	20.80	[121]
[EMIM]I	Work Function Optimization	FTO/[EMIM]I/C60/[EMIM]I/ CH$_3$NH$_3$PbI$_3$/Spiro-OMeTAD/Au	22.56	0.93	60.29	14.59	[122]
[BMIM]BF$_4$	Work Function Optimization	ITO/SnO$_2$/BMIMBF$_4$/ CH$_3$NH$_3$PbI$_3$/Spiro-OMeTAD/Au	22.90	0.945	55.00	12.1	[123]
[EMIM]PF$_6$	Work Function Optimization	FTO/ZnO/[EMIM]PF$_6$/MAPbI$_3$/Spiro- OMeTAD/Au	19.16	0.99	70.60	13.50	[40]
MAAC	Work Function Optimization	ITO/MAPbI$_3$/Spiro-OMeTAD/Au	22.40	1.15	81.6	21.08	[90]
BMIMPF$_6$	Work Function Optimization	FTO/TiO$_2$/BMIMBF$_6$/CsPbI$_2$Br/carbon	14.33	1.22	75.27	13.19	[32]

4.2. Interface Passivation

Processing of the PSCs contributes to accumulation of defects at the interfaces of each layer structure, resulting in non-radiative recombination.[124,125] In order to improve these defects, interface passivation has been used as an interface engineering strategy.[126,127] ILs as effective interfacial modifiers are viable candidates for interface passivation as they could limit the non-radiative recombination losses and thus improve the device performance.[128,129] Salado et al.[115] applied the IL imidazolium iodide (ImI) to the perovskite surface to optimize charge extraction and passivate the defects (Figure 6a,b). Owing to the large volume of imidazole

cation in ImI, the additive could not diffuse in the interior of the perovskite lattice and remained an ionic passivator to passivate the perovskite surface. Taking advantage of the passivation by ImI, long carrier lifetime, blue shifting of the perovskite emission and lower interface layer resistance were observed, which effectively offset the suface defects of the perovskite film, thereby resulting to reduced carrier recombination. The passivated device showed Jsc of 22.02 mA/cm2, a FF of 81.3% and a Voc of 1.109 V, leading to overall PCE of 19.9%. Furthermore, it is worth noting that the passivation of IL with appropriate concentration at the interface was beneficial to the device stability because of the filling effect the additive has on grain boundaries and crystals defects.

Another IL, namely 1-butyl-2,3-dimethylimidazolium chloride ([BMMIm]Cl), was incorporated by Zhang et al.[26] on the surface of the perovskite films in $CsPbBr_3$ PSCs system to passivate the surface (Figure 6c). A passivation function of the [BMMIm]Cl on the uncoordinated Pb^{2+} or Cs^+ was proven by the results of XPS and FTIR characterizations, which revealed decreased nonradiative recombination and efficient charge-transport process. As a result, the trap state density decreases from 3.44×10^{16} cm^{-3} for the $CsPbBr_3$ devices to 1.97×10^{15} cm^{-3} for devices with [BMMIm]Cl at concentrations of 10 mg mL^{-1} based on calculations using the space charge limited current (SCLC) method. Similarly, Huang et al.[116] reported an IL, methyltrioctylammonium trifluoromethanesulfonate (MATS) as passivation layer at the interface of perovskite film to compensate for the defects. Taking advantage of the low vapor pressure, this nonvolatile IL remained within the grain boundaries and flaw of perovskites surfaceas (Figure 6d). As a result of the effective passivation by MATS, the electron extraction, charge transfer resistance and related PCE of the devices were significantly improved. The same passivation function of 1,3-dimethyl-3-imidazolium hexafluorophosphate (DMIMPF$_6$) (Figure 6e) had also been reported by Zhu et al. to compensate for defects in perovskite film and to suppress the nonradiative recombination for optimized performance of the device.[31] These ILs with imidazolium group or quaternary ammonium could not diffuse into the bulk of perovskite material, involving the formation of perovskite crystals. They mainly stayed at the grain boundaries and flaw of perovskites surfaces to passivate the defects. Combining the formation of interaction between imidazolium group or quaternary ammonium in ILs and perovskite components, the ions migration in perovskite was suppressed, leading to the enhancement of device stability. Nevertheless, the effective passivation by using IL also occurs in the electron-transport layer.

24

The IL 1-butyl-3-methylimidazolium tetrafluoroborate ([BMIM]BF$_4$) was applied to the surface of PCBM by Li et al.[103] (Figure 6f), and provided efficient passivation of the surface trap states for chager transport. Compared to poor coverage of the common material bathocuproine (BCP) in the suface of PCBM, ([BMIM]BF$_4$) showed significant improvement in the coverage for efficient filling in the PCBM pinholes and defects (Figure 6g).
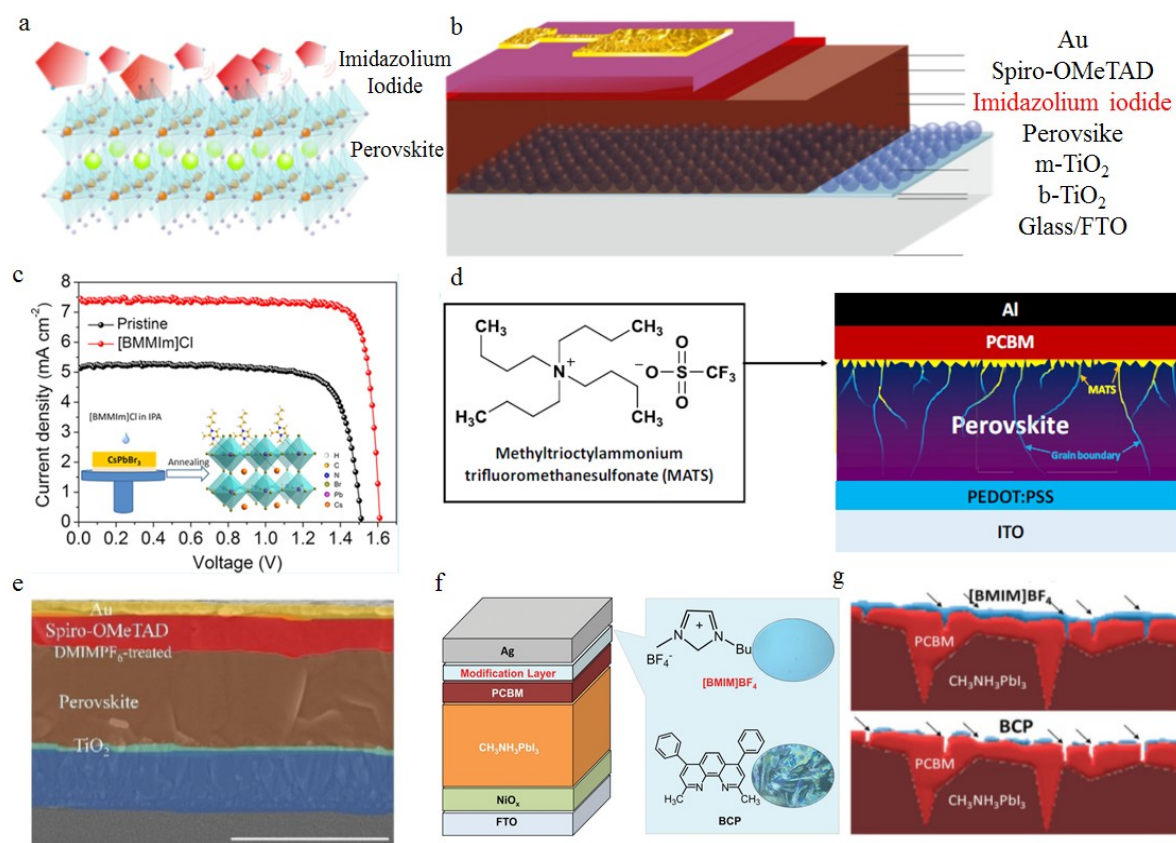
Figure 6. (a) Schematic diagram of passivation by imidazolium iodide on the surface of perovskite. (b) Structure diagram of device with imidazolium iodide as passivation layer. Copyright 2018 Elsevier Ltd.[115] (c) Schematic diagram of CsPbBr$_3$ perovskite passivation by [BMMIm]Cl IL and J–V curves of [BMMIm]Cl-treated and pristine CsPbBr$_3$ device. Copyright 2020 American Chemical Society.[26] (d) Molecular structure of MATS and schematic diagram of device structure of MATS treated planar PSCs. Copyright 2016 Elsevier B.V.[116] (e) Cross-sectional SEM images of PSCs based on DMIMPF$_6$-treated perovskite. Copyright 2020 Wiley-VCH GmbH.[31] (f) Structural representation of inverted p-i-n structure PSCs and molecule structures of [BMIM]BF$_4$ and BCP, and relevant polarized optical micro- scopic pictures. (g) Structural representation of the different passivation functions by BCP and [BMIM]BF$_4$ recombination. Copyright 2018 WILEY-VCH Verlag GmbH & Co. KGaA, Weinheim.[103]

4.2. Work Function Optimization

TiO_2 is the historically the earliest and remains the most studied electron transport layer. It is widely employed to prepare highly efficient PSCs based on its outstanding transparency and prominent stability.[130] The inferior electron mobility of TiO_2 is the most conspicuous shortcoming that limits further improvement of the device performance.[131] Moreover, the work function of TiO_2 with perovskite needs to be optimized further. Yang et al.[120] employed the IL [BMIM]BF_4 as an interface layer to the enhance electron-transport layer quality and to optimize a well-matched work function for effective improvement of electron mobility and suppression of ion migration. This provided a growth platform for high-quality perovskites, and the corresponding PSCs reached efficiency of 19.62% (Figure 7a). The work function of TiO_2 was reduced from 4.26 eV to 4.01 eV after modification of the IL, based on the Kelvin Probe Force Microscopy (KPFM) reaults. The lower work function is considered to be beneficial to reducing the return of electrons from the ETL layer to the perovskite layer, resulting in a more efficient charge transfer (Figure 7b,c). The same phenomenon of tuning the work function of TiO_2 by [BMIM]BF_4 for effective charge transfer from perovskite layer to TiO_2 has been reported by Zheng et al.[39]

SnO_2 was also considered as an option for ETL materials in planar perovskite solar cells. The energy level arrangement and the reduction of energy recombination of SnO_2-based PSCs can also be optimized by using ionic liquids.[132] Noel et al.[121] discussed the effect of different concentrations of ILs on work function, and investigated the interaction between the Ils and the perovskite layer. Different concentrations of Ils used to treat the surface of SnO_2 led to the positively related decrease of the work function owing to the emerging of a surface dipole which originates from the IL (Figure 7d,e). Interestingly, it was also found that there are significant changes of the work function of the perovskite film coming from the treated SnO_2, illustrating that the SnO_2 ETL layer treated by IL $BMIMBF_4$ also affects the electronic properties of the subsequently deposited perovskite layer.

ILs have also been used as an interface modifier to action between the C_{60} layer and the perovskite layer in n-i-p type PSCs. Xu et al.[122] modified C_{60} ETL by the IL 1-ethyl-3-methylimidazolium iodide ([EMIM]I) as an interfacial engineering approach aimed to

optimize the energy level arrangement and perovskite film. The work function of the vacant C_{60} layer decreased from 4.33 eV to 4.28 eV when [EMIM]I was deposited onto the C_{60} surface, proving the function of the IL on the reducion of the work function and regulation of the energy level arrangement (Figure 7f). The work function was conducive to electron transfer from the perovskite layer to the C_{60} layer. Morever, the IL on FTO causes decrease in the work function, leading to an efficient electron transfer from the C_{60} layer to FTO. After optimizing the work function, the relevant devices with PCE of 15.09% were obtained as n-i-p PSC structures.

Similarly, [BMIM]BF_4 was shown to be able to modify the ZnO ETL by Chu and colleagues. [123] It improves the work function and optimizes the energy level arrangement between the perovskite layer and the ETL layer, thereby facilitating efficient charge extraction. The work function of the pure ZnO and IL-treated ZnO films was determined by ultraviolet photoelectron spectrometry (UPS) to be 4.22 eV and 4.06 eV, respectively. The change in the work function of the ZnO film was caused by interfacial electric field from the IL-BF_4 molecules. This is illustrated in Figure 7g,h to indicate the adjustment of the energy level arrangement related to the increasing V_{oc} and J_{sc} in the devices. The flexible PSCs prepared based on these improvements show a PCE of 12.1%.
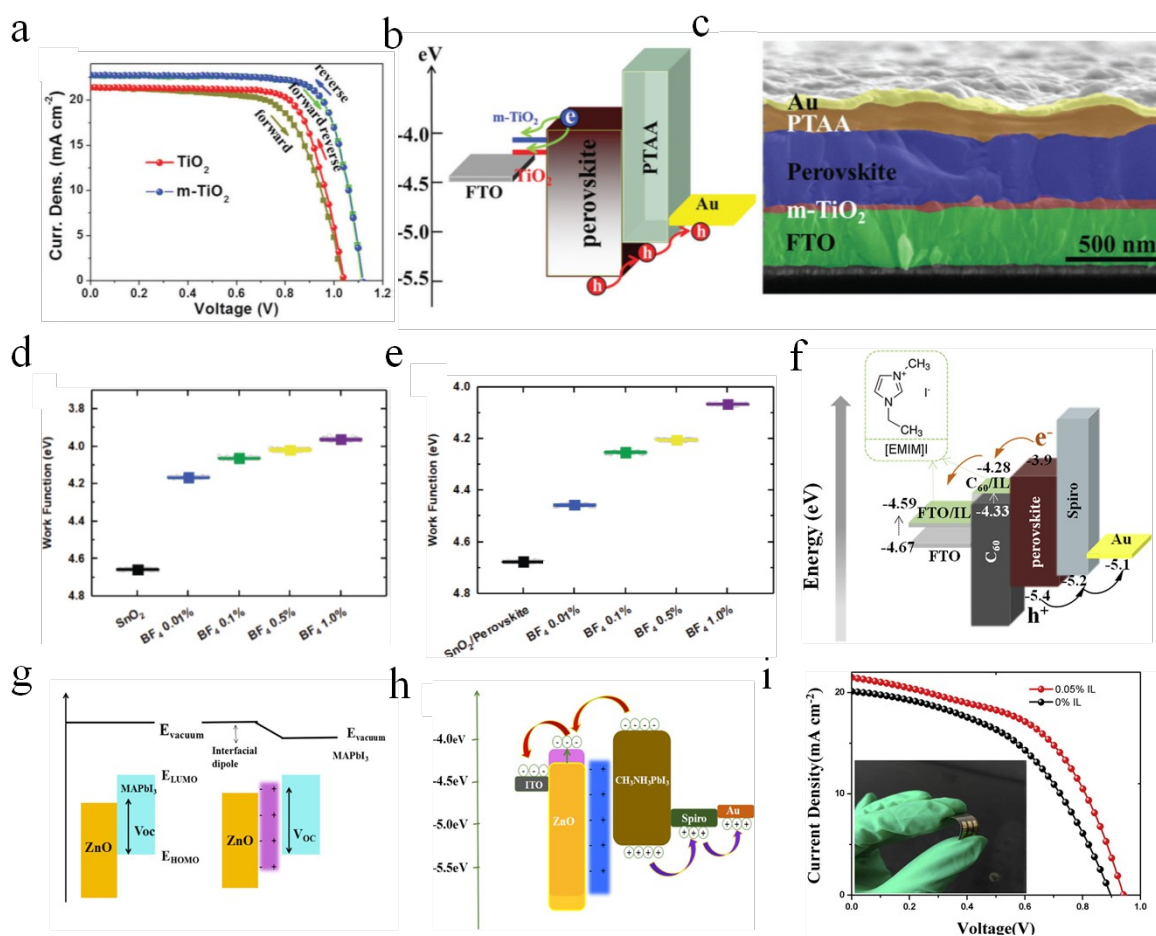
Figure 7. (a) J-V curve of PSCs based on TiO_2 and m-TiO_2 as ETL layer under both reverse and forward scan directions. (b) Schematic diagram of energy level of the PSCs. (c) Cross-sectional SEM image of the PSC device based on m-TiO_2 as ETL layer. Copyright The Royal Society of Chemistry 2016.[120] Work function of (d) SnO_2 films treated with various concentrations of BMIMBF$_4$ and (e) perovskite films deposited onto corresponding BMIMBF$_4$-treated SnO_2 films from the results of Kelvin probe measurements. Copyright 2019 WILEY-VCH Verlag GmbH & Co. KGaA, Weinheim.[121] (f) Energy level diagram of devices based on different ETLs. Copyright 2019 Published by Elsevier Inc.[122] (h) The schematic of Voc of the device based on different ETLs. (h) The energy level diagram of the devices. (i) The picture of the flexible perovskite solar cell and J-V curves of flexible PSCs with different content of ILs. Copyright 2018 Elsevier B.V.[123]

5. Stability engineering with ionic liquids

5.1. Instability of perovskite cells

After continuous optimization of the process and structure of devices based on perovskite, the efficiency of perovskite solar cells has exceeded 25%, while the efforts for improvement in the fronts of the interface engineering, composition engineering and other engineering continue.[133] In addition to efficiency of PSCs, their stability, which represents another important factor and a mandatory requirement for eventual commercialization of perovskite solar cells, has been also attended in an academic and industrial research.[134] In an actual application at varying environmental conditions, the decerase of the device effiiency caused by environmental impact or fatigue is as is important as their efficiency. The root-causes for the instability of the PSCs are mainly related to the effect of external factors such as temperature, oxygen, moisture and UV light, as well as to internal intrinsic factors including ion migration, interface defects, and interfacial reactions.[135] Many layered structures of PSC devices, such as the perovskite layer, hole transport layers and electron transport layers are indivudally affected by these factors, which normally alleviate the stability of the whole device.[136] Fortunately, ILs were developed and used to increase the stability of the PSCs through extensive structural design and location selection in devices.[62,137,138] Recent advances in the application of ionic liquids to improve the humidity stability and thermal stability of PSCs are summarized in Table 4.

Table 4. Summary of the photovoltaic parameters of PSCs with ILs in stability engineering

ILs	Function	Perovskite	Stability	Jsc (mA/cm^2)	Voc (V)	FF (%)	PCE (%)	ref
MA$^+$CF$_3$COO$^-$, MA$^+$TFA$^-$	Humidity stability	MAPbI$_3$	80±5% RH, 300 h 80% of PCE	22.70	1.15	77.10	20.10	[54]
APMimPF$_6$	Humidity stability	C$_7$H$_{15}$N$_3$BrHI	57% RH, 40 days, 98% of PCE	22.90	1.05	71.95	17.30	[139]
HMII	Humidity stability	FAPbI$_3$	60 ± 10% RH, 250 h 80% of PCE	24.85	1.07	78.00	20.6	[48]
[bvbim]Cl	Humidity stability	MAPbI$_3$	45±5% RH, 1000 h 90% of PCE	22.57	1.12	79.00	19.92	[137]
BMIMBF$_4$	Humidity stability	CsPbI$_2$Br	35% RH, 500 h 82% of PCE	17.11	1.07	72.15	13.21	[140]
RATZ	Humidity stability	MAPbI$_3$	80±5% RH, 300 h, 80% of PCE	23.39	1.10	77.84	20.03	[62]
BMIMBF$_4$	Thermal stability	(FA$_{0.83}$MA$_{0.17}$)$_{0.95}$Cs$_{0.05}$Pb(I$_{0.9}$Br$_{0.1}$)$_3$	60–65 °C, 100 h, 86% of PCE	23.80	1.08	81.00	19.80	[141]

				J_{sc}	V_{oc}	FF	PCE	
BMIBr	Thermal stability	MAPbI$_3$	85 °C, 20 min, 85% of PCE	16.90	0.96	65.00	10.55	[142]
BAAc	Thermal stability	FASnI$_3$	85 °C, 400 h, 80% of PCE	22.22	0.65	71.60	10.40	[143]
[BMP]$^+$[BF$_4$]$^-$	Thermal stability	Cs$_{0.17}$FA$_{0.83}$Pb(I$_{0.90}$Br$_{0.10}$)$_3$	85°C, 700 h, 80% of PCE	19.50	1.16	77.00	17.30	[144]
poly-RTMS	Thermal stability	Cs$_{0.05}$(MA$_{0.15}$FA$_{0.85}$)$_{0.95}$Pb(I$_{0.85}$Br$_{0.15}$)$_3$	70-75 °C 1200 h 92% of PCE	23.48	1.10	83.12	21.47	[145]
FIm	Humidity stability	Cs$_{0.05}$(MA$_{0.15}$FA$_{0.85}$)$_{0.95}$Pb(I$_{0.85}$Br$_{0.15}$)$_3$	50–55% RH. 100days excee 90% of PCE	21.69	1.00	75.19	16.32	[146]
[Bcim][TFSI]	Humidity stability	(Cs$_{0.08}$FA$_{0.8}$MA$_{0.12}$)Pb(I$_{0.88}$Br$_{0.12}$)$_3$	20–30% RH. 150days 87.9% of PCE	22.97	1.12	81.80	21.06	[38]
MA$^+$DFA$^-$	Thermal stability	MAPbI$_3$	85°C, 120 h, 80% of PCE	23.11	1.11	83.55	21.46	[138]
ETI	Humidity stability	MAPbI$_3$	40 ± 5% RH, 700 h	22.70	1.08	79.60	19.51	[20]

5.2. Stability towards humidity

Humidity, as one of the main factors to affect the stability of PSCs, often leads to irreversible degradation, which seriously affects the service life of the device. Using the principles of chemical design, hydrophobic groups in ILs were introduced to reduce the sensitivity to humidity and to overcome the effects of humidity. Liu et al.[54] introduced the IL methylammoniumtrifluoroacetate (MA$^+$CF$_3$COO$^-$, MA$^+$TFA$^-$) containing multiple fluorocarbon hydrophobic groups into a perovskite precursor solution to regulate the hydrophobicity of a perovskite film, and accomplished improvement of humidity stability. On account of the function of the hydrophobic groups, the variation of the wetting of the precursor solution caused decrease of heterogeneous nucleation, which promoted the formation of perovskite films with large grain size (Figure 8a). Consequently, perovskite films and corresponding devices showed excellent stability under high humidity. The IL-functionalized PSCs realized little damping of only 11% in 40% humidity after 336 h, which is superior to the damping of 38% for the control PSCs under identical storage conditions. Another novel IL, 3-(3-aminopropyl)-1-methylimidazolium hexafluorophosphate (APMimPF$_6$), with excellent hydrophobicity was reported by Wang and colleagues[139] to effectively enhance long-term humidity stability and maintain 98% of its original value in atmosphere with a relative humidity of 57% for 40 days. The interaction between APMimPF$_6$ and PbI$_2$, and the participation in formation of C$_7$H$_{16}$N$_3$PbI$_3$PF$_6$ by hydrophobic APMimPF$_6$

are shown in Figure 8b. These ILs were added into the perovskite precursor solution as an additive. Due to the characteristics of low volatility, ILs with hydrophobic groups will exist on the surface of the perovskite film or chemically interact with the perovskite after annealing, so as to provide hydrophobicity for improved humidity stability.

Based on the same principle, 1-hexyl-3-methylimidazolium iodide (HMII) IL was selected and introduced into a perovskite precursor solution by Akin et al.[48] to provide hydrophobicity, which was conducive to significantly improve the humidity stability of perovskite solar cells (Figure 8c). Owing to the high hydrophobicity of the long alkyl chain in HMII, the peaks of non-perovskite δ phase were not detected in HMII-treated perovskite films in an atmosphere with relative humidity (RH) of about $60 \pm 10\%$ by X-ray diffraction. This result illustrates the excellent stability of the perovskite films to humidity, leading to prevention of decomposition of the black α phase. As a reasult, the relevant devices with IL maintain over 60% of their initial efficiency after 250 h in 60% RH, whereas the control devices decay to 70% of initial efficiencies after 30 h (Figure 8d). Similarly, Xia et al.[137] proposed a new strategy to introduce a hydrophobic group in perovskite film through in situ polymerization of 1,3-bis(4-vinylbenzyl)imidazolium chloride ([bvbim]Cl), which brought about long-term stability (Figure 8e). There were unconspicuous diffraction peaks from PbI_2 in IL-treated perovskite film under humid environment in the X-ray diffraction pattern and a non-significant increase of the peak in the 350–400 nm regions for IL-treated perovskite film in the UV–vis absorption spectrum, which was taken as an evidence for the strong resistance toward decomposition by the hydrophobic crosslinked polymer in high humidity. Based on these results, PSCs were prepared in an environment of 50% RH with PCE values of 19.9%. Moreover, non-encapsulated PSCs were found to retain over 80% of their initial performance at storage environment of 45% RH after more than 2900 h.

Ionic liquids can also be employed as the interface modified layer to improve the hydrophobicity of the perovskite layer in order to improve the resistance to humidity. Wang et al.[140] proposed 1-butyl-3-methylimidazolium tetrafluoroborate (BMIMBF₄) to modify the surface of the perovskite for increased hydrophobicity and improvement of the $CsPbI_2Br$ phase stabilization. The contact angle was first conducted to investigate the hydrophobicity of the perovskite surface modified by the IL, and the angle result showed an obvious change from 30.6º to 68.5º, indicating that the interface becomes more hydrophobic to the benefit of

resisting water penetration. The change in film surface hydrophobicity had a positive effect on the phase stability of $CsPbI_2Br$. It was observed that the IL-modified perovskite film remain in the black phase at 50% RH, while the reference film faded to yellow color, as shown in Figure 8f. The phase transition from the black perovskite phase (α) to the yellow non-perovskite phase (δ) in the X-ray diffraction further confirmed that the ILs-treated perovskite films show better stability in humid environment (Figure 8g). Ultimately, a device based on $BMIMBF_4$-treated perovskite film retained 82% of initial PCE after 500 h at 35% RH. Except by directly providing hydrophobic groups by these ionic liquids, Wang and colleagues[62] invented a method to obtain hydrophobic perovskite interface through a vertical alignment of alkyl chains self-assembled of water-soluble 1-alkyl-4-amino-1,2,4-triazolium (RATZ) IL along the surface of perovskite films (Figure 8h). The obvious increase in contact angle showed that the hydrophobicity of the perovskite surface was enhanced, which was conducive to increased ability to resist humidity and prolonged service life in humid environment.
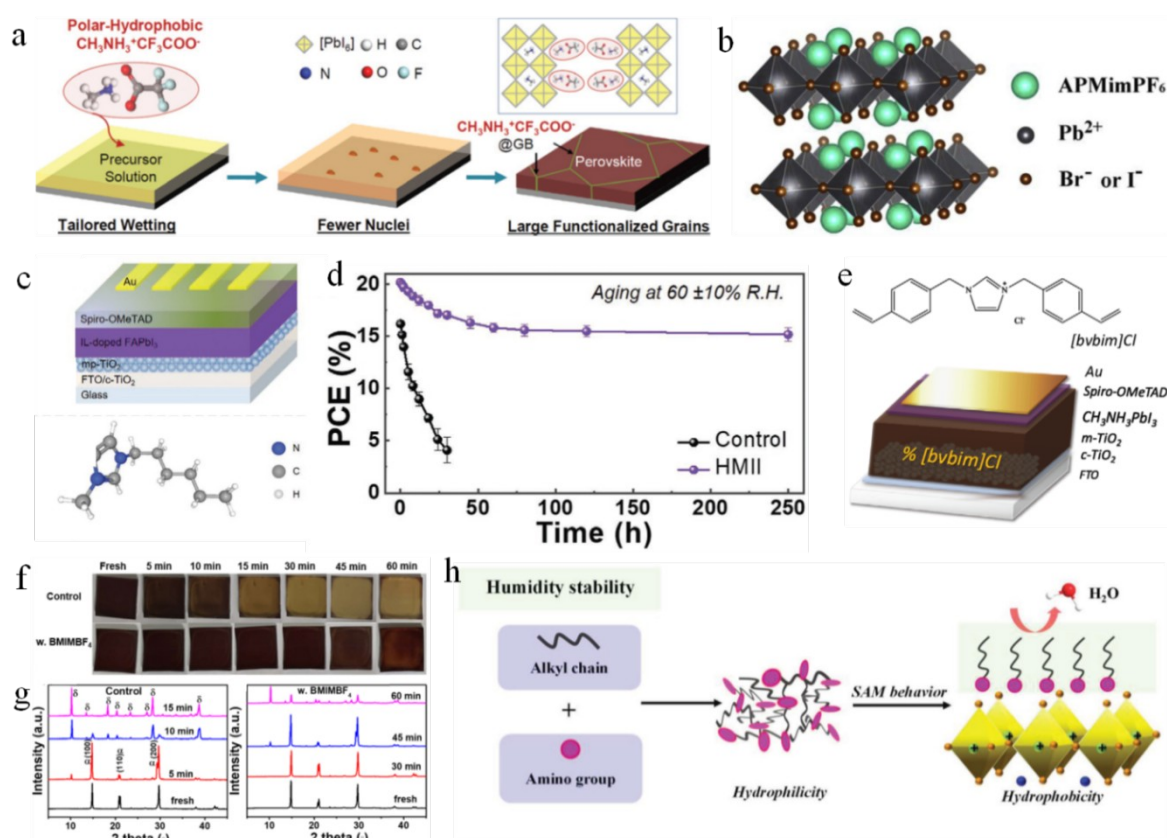
Figure 8. (a) Structural diagram of the function of hydrophobic $MA^+CF_3COO^-$ ionic liquid on $MAPbI_3$ perovskite thin films. Copyright The Royal Society of Chemistry 2019.[54] (b) Structural representation of perovskite structure based on $APMimPF_6$-HI ionic liquid. Copyright 2019 Elsevier Ltd.[139] (c) Schematic illustration of devices based on HMI^+ and chemistry structure of the HMI^+. (d) Stability curve of the devices in temperature of 25 °C and

R.H. 60 ± 10%. Copyright 2020 WILEY-VCH Verlag GmbH & Co. KGaA, Weinheim.[48] (e) Structure diagram of PSCs and chemical structure of [bvbim]Cl. Copyright 2020 Wiley-VCH GmbH.[137] (f) The pictures of control and BMIMBF$_4$-treated film in annealing process. (g) XRD patterns of the control and BMIMBF$_4$-treated perovskite films in 30 °C and 50% relative humidity. Copyright 2020 Elsevier Ltd.[140] (h) Schematic diagram of the function of triazolium ILs on the humidity stability. Copyright 2019 WILEY-VCH Verlag GmbH & Co. KGaA, Weinheim.[62]

5.3. Thermal stability

As another important factor that affects the stability of PSCs, temperature has inspired sizeable research efforts.[147] With methylammonium (MA)-based PSC as an example, the migration of the methylamine ions from the bulk to the crystal surface and subsequent formation of methylamine by the fleeing methylamine ions from the crystal lattice under heat is the primary reason for the thermotropic instability of MA-based PSCs.[148] In general, simply adding a protective layer was not sufficient to suppress the thermally induced instability. In recent years, researchers have found that the fixation of chemical interaction is an effective approach to improve the thermal stability of perovskite devices.[149] Chemical interaction was proven to exist between the perovskite and ionic liquids due to the opportunity for structural variation of the ILs.[20] Modification with different functional groups in ILs molecules is working as the most facile and direct method for chemical adjustment of ILs, which has been widely applied to meet the acquisition of the desired structure of ILs. For example, the functionalized ILs with the electron-withdrawing C=O group which are enabled with the ability to coordinate with Pb^{2+}, leading to the effective passivation of defects. The formations of hydrogen bonds between ILs with imidazolium group or quaternary ammonium and X$^-$ in perovskite materials will remarkably inhibit the migration of the X$^-$. Therefore, the modification of ILs with imidazolium group or quaternary ammonium generally enhanced stability and suppressed degeneration of PSCs device. In addition, the ILs with CH$_3$COO$^-$ were always prone to form O⋯H-N hydrogen bonds with MA$^+$ or FA$^+$ to fixed organic ions within perovskite crystal lattice.

In 2019, Bai and colleagues[141] reported an effective strategy for improving the long-term thermal stability of devices by employing 1-butyl-3-methylimidazolium tetrafluoroborate

33

(BMIMBF$_4$) as an additive to perovskite films (Figure 9a,b). It was concluded from time-of-flight secondary-ion mass spectrometry (ToF-SIMS) that BF$_4$ mainly existed at the interface of the perovskite film and BMIM dispersed throughout the film (Figure 9c,d). According to the distribution of ions and the stability experiments, by replacing BF$_4$ or BMIM the improved stability implies that the accumulated BMIM cations bind with surface sites by chemical action to suppress the degradation of the perovskite layer. As a result, the BMIMBF$_4$-modified device maintained 86% of its initial PCE at 60-65 °C in air after 100 hours and also showed longer service under full-spectrum sunlight at 70-75 °C (Figure 9e,f). Due to the diversity of anions and cations in ILs, the structure of ILs can be specifically designed by adjusting the combination of different anions and cations. The replacement of anions and anions in ILs will directly affect the both physical and chemical interaction between the ILs and perovskite precursor solution. For example, in the familiar IL BMIMBF$_4$ systems, the anion BF$_4^-$ of BMIMBF$_4$ can be replaced by the halide (X) anions, such as I$^-$, Br$^-$ or Cl$^-$. Obvious differences have been noticed for the PbI$_2$ films when ILs acted as an additive. The BMIMBF$_4$-PbI$_2$ film shows the yellowness color which is close to the pristine PbI$_2$ film, while all the other halide replaced ILs assisted PbI$_2$ films, namely BMIMI, BMIMBr and BMIMCl-PbI$_2$ films exhibit the optically transparent property, which has been explained by the formation of lead halide/imidazolium halide complexes. This research result directly evidences that the chemical 'tuning' of the IL structure upon the adjustment of anion can strongly affect the interaction between ILs and perovskite precursor solutions. For the formed complexes of PbI$_2$/BMIMX with larger band-gap, it will lead to the destruction of perovskite crystal lattice and introduce of surface strain, which seriously deteriorate the photovoltaic performance.

In another attempts to improve the thermal stability of devices by hydrogen bonding, Du et al. [142] incorporated 1-butyl-3-methylimidazolium bromine (BMIBr) into CH$_3$NH$_3$PbI$_3$ perovskite film to form interactions with the perovskite and to anchor the MA cation for increased heat resistance. Moreover, BMIBr also plays a significance role in promoting the growth of perovskite grains to form high-quality films and prevents the deterioration of MA at the grain boundaries and on the surface. A BMIBr-modified device retains 85% of its initial PCE under heating at 85 oC for 20 minutes, which is superior to a control device with the 70% of its initial PCE unde the same conditions (Figure 9g,h).

Very recently, Li et al.[143] employed the IL *n*-butylammonium acetate (BAAc) to stabilize tin halide PSCs by adjusting tin coordination with O···Sn bonds and N-H···X hydrogen bonds to inhibit the oxidation of Sn(II). The XRD measurement was conducted for BAAc-containing perovskite films to indicate that diffraction peaks along the (100) and (200) planes were maintained after heating at 85 °C in 384 h, explaining the suppression of ion migration during heating (Figure 9i). The corresponding devices showed a 80% PCE of the original after 400 h heating under 85 °C (Figure 9j). Furthermore, the strategy of retarding compositional segregation to improve the thermal stability of PSCs was regarded as another effective approach. Lin et al.[144] employed 1-butyl-1-methylpiperidinium tetrafluoroborate ([BMP]+ [BF4]−) as an additive to hinder component segregation and reduce the defects for long life PSCs (Figure 9k). The related PSCs with [BMP]+[BF4]− maintained 80% of the original PCE under full-spectrum sunlight at 60 °C after 2630 hours (Figure 9l). More surprisingly, approximately 80% of the original PCE for PSCs remianed under full-spectrum sunlight at 85 °C over 700 h (Figure 9 m).

Chen and colleagues systematically revealed the mechanism of inhibition of ion migration for PSCs with excellent stability under thermal stress or realistic operation conditions through analyzing physical barrier and chemical bonding properties after using the Poly(ionic-liquid)s (PILs) as additives.[150] Due to the existent of the chemical bonding, electrostatic interaction, and steric hindrance through the introduction of PILs additives, satisfying passivation effect on Pb defects and significantly suppression of I- ion migration were discovered. In addition, taking the advantage of the removal of residual tensile stress and the appearance of compressive strain, the activation energy of ion migration was improved for the enhanced intrinsic stability. The polymerization of ILs to from PILs is also related to the chemical mechanism adjustment of ILs. In contrast to the traditional ones, the ILs with C=C bonds can take place the polymerization under certain conditions to form PILs with multiple repetitive units. Through the adjustment of chemical structure by polymerization, the PILs possess the characteristics of highlights of both ILs and polymers, showing several properties of adaptive solubility, excellent thermal stability, and chemical durability. More importantly, the PILs with repeating units generally contain multi-site anchored groups to form a highly coordinated interaction between PILs and perovskite with strong bonding stability, which is beneficial to effectively passivate lead defects. In addition, the formed long carbon chain skeleton endows

more hydrophobic property and cooperates with highly coordination interactions to effectively improve the stability of PSCs.
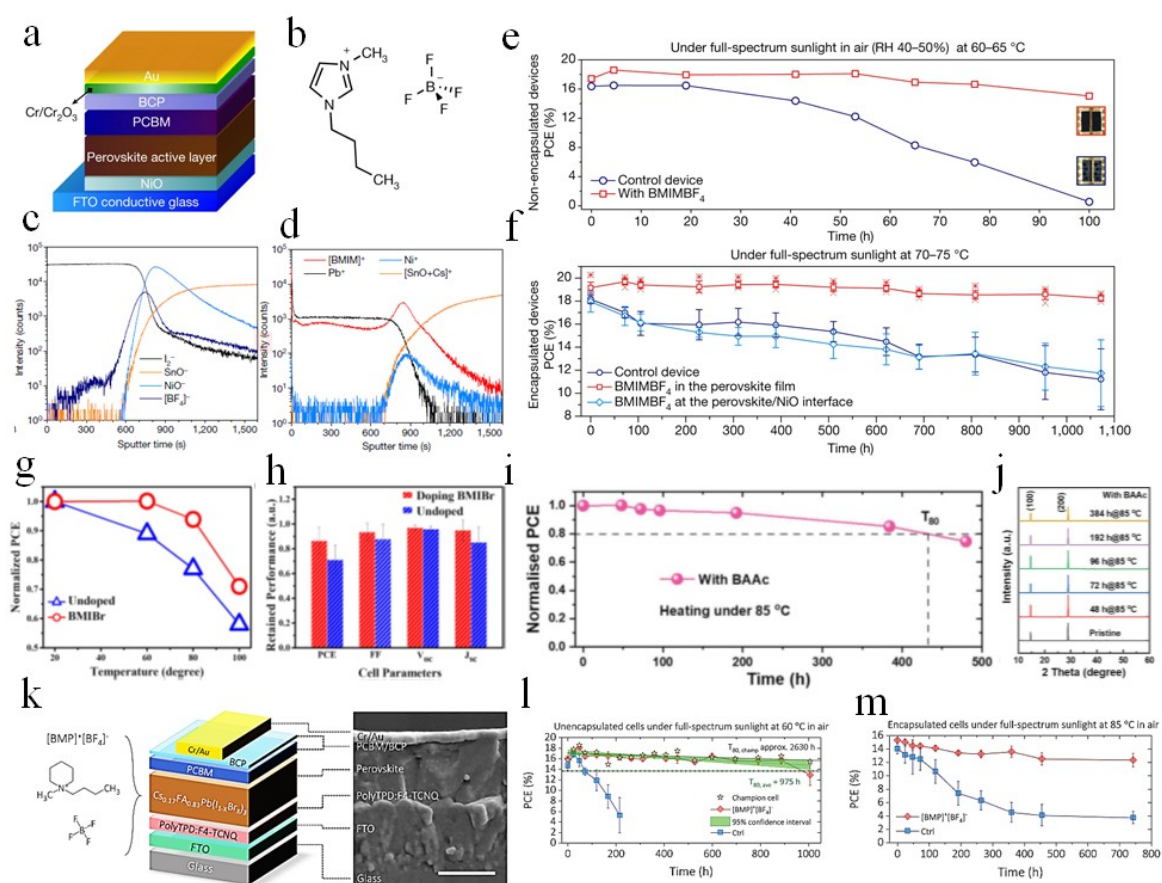
Figure 9. (a) Structural diagram of planar heterojunction positive-intrinsic-negative perovskite solar cell. (b) Chemical structure of the ionic liquid BMIMBF$_4$. (c-d) ToF-SIMS depth measurements of the BMIMBF$_4$-treated perovskite film on an NiO/FTO-coated glass substrate in negative and positive polarity. (e) Stability performance of the non-encapsulated control device and a BMIMBF$_4$-treated device under full-spectrum sunlight at 60–65 °C in air with RH ranging from 40% to 50%. (f) Stability performance of the encapsulated PSCs under full-spectrum sunlight at 70–75 °C. Copyright 2019 Springer Nature Ltd.[141] (g) The PCE variation of undoped and BMIB-treated PSCs along with heating temperature. (h) The photovoltaic parameter (PCE, FF, V$_{OC}$ and J$_{SC}$) variations of undoped and BMIB-treated PSCs after heating at 85 °C for 20 min. The error bars are from the standard deviation of ten PSCs. 2018 WILEY-VCH Verlag GmbH & Co. KGaA, Weinheim.[142] (i) Long-term thermal stability of BAAc-containing device at 85 °C inside a N$_2$-filled glovebox. (j) XRD pattern of BAAc-containing films heated at 85 °C in different times. Copyright 2021 The Authors. Advanced Energy Materials published by Wiley-VCH GmbH.[143] (k) Schematic of the p-i-n

PSCs and the molecule structure of [BMP]$^+$[BF4]$^-$. (l) Stability of unencapsulated PSCs based on $Cs_{0.17}FA_{0.83}Pb(I_{0.77}Br_{0.23})_3$ with and without 0.25 mol % [BMP]$^+$[BF4]$^-$ under full-spectrum sunlight at 60°C in ambient air. (m) Stability of unencapsulated PSCs based on $Cs_{0.17}FA_{0.83}Pb(I_{0.77}Br_{0.23})_3$ with and without 0.25 mol % [BMP]$^+$[BF4]$^-$ under full-spectrum sunlight at 85°C in ambient air (six cells for each condition). Copyright 2020 American Association for the Advancement of Science.[144]

6. Summary and outlook

In this review, we provide a comprehensive overview of the state-of-the-art application of ILs in the ever-expanding reseach of PSCs. Specifically, we address and analyze the most recent developments in understanding the role of ILs in the engineering of the perovskite precursor solution, charge transport layer, interfaces and stability aimed at the preparation of high-performance PCSs. The effect of ILs on the perovskite precursor solution engineering depends on how the ILs are used; they can be applied as additives or as a sole solvent of the perovskite precursor solution. The chemical composition of the ILs when used as additives play a critical role in the crystallization process of perovskites, and they could induce formation of larger grain perovskite crystals and more uniform perovskite films. Perhaps more surprisingly, ILs can be used as a single green solvent to replace the traditional toxic organic solvents for the preparation of PSCs with excellent performance. The selected ILs aid in the dissolution of the organic and inorganic components in perovskite precursor solutions as a result of the chemical interaction between the solute and solvent, and this provides high-quality films. Moreover, when used as a solvent, the ILs can control the crystal growth process of the perovskite to form higly crystalline, oriented films.

In the domain of charge transport layer engineering, the ILs have been used as electron and hole transport layer dopants to improve the charge mobility of the traditional transport layer materials. Taking advantage of their excellent stability and ionic conductivity, ILs were used as single electron transport layer to simplify the manufacturing process and adapt to flexible PSCs for practical applications. However, the efficiency of the PSCs based on ILs as a single transport layer is not ideal, and further development of new types of ILs is required. Moreover, we have discussed the application of ILs for work function optimization and interface passivation in interfacial engineering. The interface modification between the

traditional transport layer material and the perovskite layer is an effective way to adjust the work function and to obtain a well-matched energy level arrangement, which is beneficial to improved charge transfer. ILs are regarded as excellent interface modifiers for passivating surfaces because of their remarkable permeability and functionality. Aiming at solving the extant problem of perovskite stability, ILs were found to effectively improve the stability towards humidity as well as the thermal stability due to their hydrophobicity and chemical interaction with the perovskite components. The summary of the stability of PSCs based on various ILs will be of help to those who work in the field and will direct future research efforts. Finally, understanding systematically the principles of ILs design in the perovskite field will provide the basis for highly selecting appropriate ILs in the preparation of perovskite devices. Specifically, the selection principles are as follows:

(1) Low toxicity: Taking consideration of the green and safety, the design and selection on components of ILs with cations and anions should avoid the employment of toxic ions. Together with the non-volatile characteristics, the ILs with low structural toxicity is enabled with the great potential as substitution of volatile organic solvents and additive in commercialization of perovskite devices.

(2) Specific action mechanism: The design principles are also highly depended on the specific effect of ILs on PSCs, such as regulating crystallization, passivation, serving as solvent, adjusting energy level arrangement and improving stability. The designed ILs with the functional groups, including the hydrogen bond acceptor/donor or lone pair electrons, which can interact with perovskite precursors materials for the regulation of crystal growth and defect passivation. In order to meet the requirements of acting as solvent, the designed ILs with hydrogen bonding and Lewis acidity or alkalinity can contribute to the solubility of perovskite precursor material. In addition, if taking into consideration of ILs on the adjustment of energy level arrangement, the designed ILs should possess good energy level matching and excellent electrochemical characteristics, promoting efficient carrier collection at the interfaces of PSCs. Aimed at the improvement of the stability, the designed ILs with hydrophobic group or long alkyl chains should be designed to enhance the resistance of devices to humidity.

(3) Low synthesis cost: The design of late-model ILs should be based on the simple and low-cost process, and it is easy to repeat the synthesis steps, which matched the commercial application of perovskite devices.

(4) Preparation technology: In the traditional spin coating process, generally, selection of the ILs with high viscosity should be avoided due to increasing the viscosity of perovskite precursor solution to affect the coverage of film. Similarly, ILs with appropriate viscosity was selected in other large-area preparation processes.

Progress in the application of ILs has made huge strides towards stable, durable and efficient PSCs, and at the current stage, the ILs are considered to carry a great potential for replacing the traditionally used additives for stable PSCs. However, it should be noted that a number of challenges remain and more research is needed in this research field. Some of the immediate challenges about ILs and application in PSCs to be addressed are listed here.

The unique challenges for ILs as follow:

(1) The most prominent is that the decomposition and reaction activities of ILs should not be underestimated. Specifically, the reactivity of ILs will lead to the formation of useful or harmful reaction intermediates, resulting to the complex analysis process of application mechanism.[151] Hence, in-depth perceiving of physical and chemical properties of ILs will provide a basis for selecting appropriate ILs for perovskite devices.

(2) At present, the synthesis of late-model ionic liquids still encounter some challenges, especially in the simplification of synthesis steps and the reduction of synthesis costs.[152] Low cost and easily repeatable synthesis of ILs are suitable for a wider range of applications.

(3) The hygroscopic property of ILs is worth considering, which limited some applications of ILs. Influence will be brought on the direction of ionic liquid molecules and the electrostatic interaction between ions after exposing to water.[153]

The challenges about the application of ILs in PSCs:

1) A deeper understanding of the actual chemical interactions between the ILs and the perovskite precursor solution is needed, and this should be supplemented by in situ monitoring of the evolution of the new precursor phase in the spin-coating process. Concentrating on the specific role of the ILs in crystal nucleation and growth of perovskite crystals as well as the evolution of IL-related precursor phases(s) is foreseen as an effective means to control the formation energy of perovskites and stabilization of the desired perovskite phase(s).

2) Furthermore, the effect of residual ILs on the perovskite films is not clear. Due to their low volatility, ILs as additives often remain in the perovskite films. Some studies have implicated that these residual ILs can passivate defects or improve the stability towards aerial humidity due to the presence of hydrophobic groups. However, the interaction between the dispersion of ILs in perovskite films remains debatable.

3) Design and selection of appropriate ILs for application in high-efficient and stable PSCs is still worth considering. New types of specific ILs need to be developed to further improve the performance of the PSCs. In addition, the selectivity of ILs containing certain functional groups will surely affect the interaction between the ILs and the perovskite, which will ultimately affect the performance of devices. Understanding of the relationships between the structure and properties of ILs can effectively select the appropriate ILs for high-performance PSCs.

4) The application of ILs in large-scale preparation of perovskite solar cells through large-scale roll-to-roll and blade-coating technology is a direction that is worth exploring. In order to satisfy the practical application, ILs are to be also regarded as important materials in future large-scale production.

Received: ((will be filled in by the editorial staff))

Revised: ((will be filled in by the editorial staff))

Published online: ((will be filled in by the editorial staff))

Reference

[1]   S. Chen, Y. Deng, X. Xiao, S. Xu, P. N. Rudd, J. Huang, *Nat. Sustain.* **2021**, *4*, 636.

[2]   Q. Zhou, Y. Gao, C. Cai, Z. Zhang, J. Xu, Z. Yuan, P. Gao, *Angew. Chemie Int. Ed.* **2021**, *60*, 8303.

[3]   P. Ahlawat, A. Hinderhofer, E. A. Alharbi, H. Lu, A. Ummadisingu, H. Niu, M. Invernizzi, S. M. Zakeeruddin, M. I. Dar, F. Schreiber, A. Hagfeldt, M. Grätzel, U. Rothlisberger, M. Parrinello, *Sci. Adv.* **2021**, *7*, eabe3326.

[4]   C. Liang, D. Zhao, Y. Li, X. Li, S. Peng, G. Shao, G. Xing, *Energy Environ. Mater.* **2018**, *1*, 221.

[5]   W. Li, M. U. Rothmann, Y. Zhu, W. Chen, C. Yang, Y. Yuan, Y. Y. Choo, X. Wen, Y.-B. Cheng, U. Bach, J. Etheridge, *Nat. Energy* **2021**, *6*, 624.

[6]   N. Li, X. Niu, L. Li, H. Wang, Z. Huang, Y. Zhang, Y. Chen, X. Zhang, C. Zhu, H. Zai, Y. Bai, S. Ma, H. Liu, X. Liu, Z. Guo, G. Liu, R. Fan, H. Chen, J. Wang, Y. Lun, X. Wang, J. Hong, H. Xie, D. S. Jakob, X. G. Xu, Q. Chen, H. Zhou, *Science.* **2021**, *373*, 561.

[7]   H. Min, D. Y. Lee, J. Kim, G. Kim, K. S. Lee, J. Kim, M. J. Paik, Y. K. Kim, K. S. Kim, M. G. Kim, T. J. Shin, S. Il Seok, *Nature* **2021**, *598*, 444.

[8]   W.-Q. Wu, J.-F. Liao, J.-X. Zhong, Y.-F. Xu, L. Wang, J. Huang, *Angew. Chemie Int. Ed.* **2020**, *59*, 20980.

[9]   H. Li, G. Wu, W. Li, Y. Zhang, Z. Liu, D. Wang, S. (Frank) Liu, *Adv. Sci.* **2019**, *6*, 1901241.

[10]   G. Kim, H. Min, K. S. Lee, D. Y. Lee, S. M. Yoon, S. Il Seok, *Science.* **2020**, *370*, 108.

[11]   L. Chao, T. Niu, W. Gao, C. Ran, L. Song, Y. Chen, W. Huang, *Adv. Mater.* **2021**, *33*, 2005410.

[12]   F. Zhang, K. Zhu, *Adv. Energy Mater.* **2020**, *10*, 1902579.

[13]   S. Liu, Y. Guan, Y. Sheng, Y. Hu, Y. Rong, A. Mei, H. Han, *Adv. Energy Mater.* **2020**, *10*, 1902492.

[14]   J. Zhu, D. H. Kim, J. D. Kim, D. G. Lee, W. Bin Kim, S. wang Chen, J. Y. Kim, J. M. Lee, H. Lee, G. S. Han, T. K. Ahn, H. S. Jung, *ACS Energy Lett.* **2021**, *6*, 3425.

[15]   L. Caliò, M. Salado, S. Kazim, S. Ahmad, *Joule* **2018**, *2*, 1800.

[16]   Q. Jiang, Y. Zhao, X. Zhang, X. Yang, Y. Chen, Z. Chu, Q. Ye, X. Li, Z. Yin, J. You, *Nat. Photonics* **2019**, *13*, 460.

[17]   S. H. Turren-Cruz, A. Hagfeldt, M. Saliba, *Science.* **2018**, *362*, 449.

[18]   A. Mahapatra, D. Prochowicz, M. M. Tavakoli, S. Trivedi, P. Kumar, P. Yadav, *J. Mater. Chem. A* **2020**, *8*, 27.

[19]   T. Niu, L. Chao, W. Gao, C. Ran, L. Song, Y. Chen, L. Fu, W. Huang, *ACS Energy Lett.* **2021**, *6*, 1453.

[20]   R. Xia, Z. Fei, N. Drigo, F. D. Bobbink, Z. Huang, R. Jasiūnas, M. Franckevičius, V. Gulbinas, M. Mensi, X. Fang, C. Roldán-Carmona, M. K. Nazeeruddin, P. J. Dyson, *Adv. Funct. Mater.* **2019**, *29*, 1902021.

[21]   P. Wasserscheid, W. Keim, *Angew. Chem. Int. Ed* **2000**, *39*, 3772.

[22]   S. Ghosh, T. Singh, *Nano Energy* **2019**, *63*, 103828.

[23]   C. Luo, G. Li, L. Chen, J. Dong, M. Yu, C. Xu, Y. Yao, M. Wang, Q. Song, S. Zhang, *Sustain. Energy Fuels* **2020**, *4*, 3971.

[24]   P. Caprioglio, D. S. Cruz, S. Caicedo-Dávila, F. Zu, A. A. Sutanto, F. Peña-Camargo, L. Kegelmann, D. Meggiolaro, L. Gregori, C. M. Wolff, B. Stiller, L. Perdigón-Toro, H. Köbler, B. Li, E. Gutierrez-Partida, I. Lauermann, A. Abate, N. Koch, F. De Angelis, B. Rech, G. Grancini, D. Abou-Ras, M. K. Nazeeruddin, M. Stolterfoht, S. Albrecht, M. Antonietti, D. Neher, *Energy Environ. Sci.* **2021**, *14*, 4508.

[25]   X. Xia, J. Peng, Q. Wan, X. Wang, Z. Fan, J. Zhao, F. Li, *ACS Appl. Mater. Interfaces* **2021**, *13*, 17677−17689.

[26]   W. Zhang, X. Liu, B. He, Z. Gong, J. Zhu, Y. Ding, H. Chen, Q. Tang, *ACS Appl. Mater. Interfaces* **2020**, *12*, 4540.

[27]   S. Öz, J. Burschka, E. Jung, R. Bhattacharjee, T. Fischer, A. Mettenbörger, H. Wang, S. Mathur, *Nano Energy* **2018**, *51*, 632.

[28]   N. Cho, F. Li, B. Turedi, L. Sinatra, S. P. Sarmah, M. R. Parida, M. I. Saidaminov, B. Murali, V. M. Burlakov, A. Goriely, O. F. Mohammed, T. Wu, O. M. Bakr, *Nat. Commun.* **2016**, *7*, 13407.

[29]   Y. Xia, C. Ran, Y. Chen, Q. Li, N. Jiang, C. Li, Y. Pan, T. Li, J. P. Wang, W. Huang, *J. Mater. Chem. A* **2017**, *5*, 3193.

[30]   L. Liu, Z. Tang, C. Xin, S. Zhu, S. An, N. Wang, L. Fan, C. Wei, Q. Huang, G. Hou, Y. Zhao, Y. Ding, X. Zhang, *ACS Appl. Energy Mater.* **2018**, *1*, 2730.

[31]   X. Zhu, M. Du, J. Feng, H. Wang, Z. Xu, L. Wang, S. Zuo, C. Wang, Z. Wang, C. Zhang, X. Ren, S. Priya, D. Yang, S. F. Liu, *Angew.Chem. Int. Ed.* **2021**, *16802*, 4238.

[32] R. Yin, K.-X. Wang, S. Cui, B.-B. Fan, J.-W. Liu, Y.-K. Gao, T.-T. You, P.-G. Yin, *ACS Appl. Energy Mater.* **2021**, *4*, 9294.

[33] O. Nordness, J. F. Brennecke, *Chem. Rev.* **2020**, *120*, 12873.

[34] M. T. Hoang, N. D. Pham, Y. Yang, V. T. Tiong, C. Zhang, K. Gui, H. Chen, J. Chang, J. Wang, D. Golberg, J. Bell, H. Wang, *Green Chem.* **2020**, *22*, 3433.

[35] J. Xu, J. Cui, S. Yang, Y. Han, X. Guo, Y. Che, D. Xu, C. Duan, W. Zhao, K. Guo, W. Ma, B. Xu, J. Yao, Z. Liu, S. Liu, *Nano-Micro Lett.* **2022**, *14*, 7.

[36] N. Wei, Y. Chen, X. Wang, Y. Miao, Z. Qin, X. Liu, H. Wei, Y. Zhao, *Adv. Funct. Mater.* **2021**, 2108944.

[37] Y. Du, Q. Tian, X. Chang, J. Fang, X. Gu, X. He, X. Ren, K. Zhao, S. Liu, *Adv. Mater.* **2022**, 2106750.

[38] X. X. Gao, B. Ding, H. Kanda, Z. Fei, W. Luo, Y. Zhang, N. Shibayama, A. Züttel, F. F. Tirani, R. Scopelliti, S. Kinge, B. Zhang, Y. Feng, P. J. Dyson, M. K. Nazeeruddin, *Cell Reports Phys. Sci.* **2021**, *2*, 100475.

[39] X. Zheng, W. Yu, S. Priya, *J. Energy Chem.* **2018**, *27*, 748.

[40] W. Zhang, Z. Ren, Y. Guo, X. He, X. Li, *Electrochim. Acta* **2018**, *268*, 539.

[41] S. Wang, H. Chen, J. Zhang, G. Xu, W. Chen, R. Xue, M. Zhang, Y. Li, Y. Li, *Adv. Mater.* **2019**, *31*, 1903691.

[42] H. Hu, Z. Ren, P. W. K. Fong, M. Qin, D. Liu, D. Lei, X. Lu, G. Li, *Adv. Funct. Mater.* **2019**, *29*, 1900092.

[43] L. Xie, J. Chen, P. Vashishtha, X. Zhao, G. S. Shin, S. G. Mhaisalkar, N.-G. Park, *ACS Energy Lett.* **2019**, *4*, 2192.

[44] J. Y. Seo, T. Matsui, J. Luo, J. P. Correa-Baena, F. Giordano, M. Saliba, K. Schenk, A. Ummadisingu, K. Domanski, M. Hadadian, A. Hagfeldt, S. M. Zakeeruddin, U. Steiner, M. Grätzel, A. Abate, *Adv. Energy Mater.* **2016**, *6*, 1600767.

[45] Y. Zhang, Z. Fei, P. Gao, Y. Lee, F. F. Tirani, R. Scopelliti, Y. Feng, P. J. Dyson, M. K. Nazeeruddin, *Adv. Mater.* **2017**, *29*, 1702157.

[46] Y. Wu, F. Xie, H. Chen, X. Yang, H. Su, M. Cai, Z. Zhou, T. Noda, L. Han, *Adv. Mater.* **2017**, *29*, 1701073.

[47] T. Li, S. Wang, J. Yang, X. Pu, B. Gao, Z. He, Q. Cao, J. Han, X. Li, *Nano Energy* **2021**, *82*, 105742.

[48] S. Akin, E. Akman, S. Sonmezoglu, *Adv. Funct. Mater.* **2020**, *30*, 2002964.

[49] D. Huang, P. Xie, Z. Pan, H. Rao, X. Zhong, *J. Mater. Chem. A* **2019**, *7*, 22420.

[50] Y. Wan, S. Dong, Y. Wang, L. Yang, W. Qin, H. Cao, C. Yao, Z. Ge, S. Yin, *RSC Adv.* **2016**, *6*, 97848.

[51] M. Shahiduzzaman, K. Yamamoto, Y. Furumoto, T. Kuwabara, K. Takahashi, T. Taima, *RSC Adv.* **2015**, *5*, 77495.

[52] M. Shahiduzzaman, K. Yamamoto, Y. Furumoto, K. Yonezawa, K. Hamada, K. Kuroda, K. Ninomiya, M. Karakawa, T. Kuwabara, K. Takahashi, K. Takahashi, T. Taima, *Org. Electron.* **2017**, *48*, 147.

[53] R. Xu, H. Dong, P. Li, X. Cao, H. Li, J. Li, Z. Wu, *ACS Appl. Mater. Interfaces* **2021**, *13*, 33218.

[54] D. Liu, Z. Shao, J. Gui, M. Chen, M. Liu, G. Cui, S. Pang, Y. Zhou, *Chem. Commun.* **2019**, *55*, 11059.

[55] X. Zhou, Y. Wang, C. Li, T. Wu, *Chem. Eng. J.* **2019**, *372*, 46.

[56] Z. Lin, Y. Su, R. Dai, G. Liu, J. Yang, W. Sheng, Y. Zhong, L. Tan, Y. Chen, *ACS Appl. Mater. Interfaces* **2021**, *13*, 15420−15428.

[57] C. Sun, Q. Xue, Z. Hu, Z. Chen, F. Huang, H. L. Yip, Y. Cao, *Small* **2015**, *11*, 3344.

[58] P. Chen, Y. Zhang, J. Du, Y. Wang, X. Zhang, Y. Liu, *J. Phys. Chem. C* **2018**, *122*, 10699.

[59] Y. Xiao, L. Yang, G. Han, Y. Li, M. Li, H. Li, *Org. Electron.* **2019**, *65*, 201.

[60] L. Yang, X. Ma, X. Shang, D. Gao, C. Wang, M. Li, C. Chen, B. Zhang, S. Xu, S. Zheng, H. Song, *Sol. RRL* **2021**, *5*, 2100352.

[61] C. Liang, H. Gu, Y. Xia, Z. Wang, X. Liu, J. Xia, S. Zuo, Y. Hu, X. Gao, W. Hui, L. Chao, T. Niu, M. Fang, H. Lu, H. Dong, H. Yu, S. Chen, X. Ran, L. Song, B. Li, J. Zhang, Y. Peng, G. Shao, J. Wang, Y. Chen, G. Xing, W. Huang, *Nat. Energy* **2021**, *6*, 38.

[62] S. Wang, Z. Li, Y. Zhang, X. Liu, J. Han, X. Li, Z. Liu, S. (Frank) Liu, W. C. H. Choy, *Adv. Funct. Mater.* **2019**, *29*, 1900417.

[63] M. Shahiduzzaman, L. Wang, S. Fukaya, E. Y. Muslih, A. Kogo, M. Nakano, M. Karakawa, K. Takahashi, K. Tomita, J. M. Nunzi, T. Miyasaka, T. Taima, *ACS Appl. Mater. Interfaces* **2021**, *13*, 21194.

[64] W. Zhang, J. Du, C. Qiu, K. Yang, Q. Huang, Q. Wang, W. Zhang, H. Han, X. Gao, Y. Hu, *Chem. Commun.* **2021**, *57*, 4027.

[65]   D. T. Moore, K. W. Tan, H. Sai, K. P. Barteau, U. Wiesner, L. A. Estroff, *Chem. Mater.* **2015**, *27*, 3197.

[66]   W. Hui, L. Chao, H. Lu, F. Xia, Q. Wei, Z. Su, T. Niu, L. Tao, B. Du, D. Li, Y. Wang, H. Dong, S. Zuo, B. Li, W. Shi, X. Ran, P. Li, H. Zhang, Z. Wu, C. Ran, L. Song, G. Xing, X. Gao, J. Zhang, Y. Xia, Y. Chen, W. Huang, *Science.* **2021**, *371*, 1359.

[67]   L. Chao, Y. Xia, B. Li, G. Xing, Y. Chen, W. Huang, *Chem* **2019**, *5*, 995.

[68]   X. Wang, X. Ran, X. Liu, H. Gu, S. Zuo, W. Hui, H. Lu, B. Sun, X. Gao, J. Zhang, Y. Xia, Y. Chen, W. Huang, *Angew. Chemie Int. Ed.* **2020**, *59*, 13354.

[69]   L. Chao, T. Niu, H. Gu, Y. Yang, Q. Wei, Y. Xia, W. Hui, S. Zuo, Z. Zhu, C. Pei, X. Li, J. Zhang, J. Fang, G. Xing, H. Li, X. Huang, X. Gao, C. Ran, L. Song, L. Fu, Y. Chen, W. Huang, *Research* **2020**, *2020*, 2616345.

[70]   S. Lv, W. Gao, C. Ran, D. Li, L. Chao, X. Wang, L. Song, Z. Lin, L. Fu, Y. Chen, *Sol. RRL* **2021**, *5*, 2100675.

[71]   H. Ren, S. Yu, L. Chao, Y. Xia, Y. Sun, S. Zuo, F. Li, T. Niu, Y. Yang, H. Ju, B. Li, H. Du, X. Gao, J. Zhang, J. Wang, L. Zhang, Y. Chen, W. Huang, *Nat. Photonics* **2020**, *14*, 154.

[72]   L. Gu, C. Ran, L. Chao, Y. Bao, W. Hui, Y. Wang, Y. Chen, X. Gao, L. Song, *ACS Appl. Mater. Interfaces* **2021**, In press.

[73]   Q. Jiang, Z. Chu, P. Wang, X. Yang, H. Liu, Y. Wang, Z. Yin, J. Wu, X. Zhang, J. You, *Adv. Mater.* **2017**, *29*, 1703852.

[74]   Z. Liu, F. Cao, M. Wang, M. Wang, L. Li, *Angew. Chemie Int. Ed.* **2020**, *59*, 4161.

[75]   D. T. Moore, H. Sai, K. W. Tan, D. M. Smilgies, W. Zhang, H. J. Snaith, U. Wiesner, L. A. Estroff, *J. Am. Chem. Soc.* **2015**, *137*, 2350.

[76]   S. Yang, Y. C. Zheng, Y. Hou, X. Chen, Y. Chen, Y. Wang, H. Zhao, H. G. Yang, *Chem. Mater.* **2014**, *26*, 6705.

[77]   H. Zhang, M. Qin, Z. Chen, W. Yu, Z. Ren, K. Liu, J. Huang, Y. Zhang, Q. Liang, H. T. Chandran, P. W. K. Fong, Z. Zheng, X. Lu, G. Li, *Adv. Mater.* **2021**, *33*, 2100009.

[78]   J. G. Tait, T. Merckx, W. Li, C. Wong, R. Gehlhaar, D. Cheyns, M. Turbiez, P. Heremans, *Adv. Funct. Mater.* **2015**, *25*, 3393.

[79]   E. Rezaee, W. Zhang, S. R. P. Silva, *Small* **2021**, *17*, 2008145.

[80]   M. Zhang, D. Xin, X. Zheng, Q. Chen, W. H. Zhang, *ACS Sustain. Chem. Eng.* **2020**, *8*, 13126.

[81] H. Gu, T. Niu, S. Zuo, Y. Cai, L. Chao, P. Müller-Buschbaum, Y. Xia, J. Zhang, G. Xing, Y. Chen, *CCS Chem.* **2022**, 1.

[82] M. Cheng, C. Zuo, Y. Wu, Z. Li, B. Xu, Y. Hua, L. Ding, *Sci. Bull.* **2020**, *65*, 1237.

[83] Y. Wang, J. Wan, J. Ding, J. Hu, D. Wang, *Angew. Chemie Int. Ed.* **2019**, *131*, 9514.

[84] Q. Jiang, L. Zhang, H. Wang, X. Yang, J. Meng, H. Liu, Z. Yin, J. Wu, X. Zhang, J. You, *Nat. Energy* **2017**, *2*, 16177.

[85] C. Huang, P. Lin, N. Fu, K. Sun, M. Ye, C. Liu, X. Zhou, L. Shu, X. Hao, B. Xu, X. Zeng, Y. Wang, S. Ke, *J. Mater. Chem. A* **2018**, *6*, 22086.

[86] J. Luan, J. Xu, J. Chen, X. Shi, B. Zhang, S. Dai, J. Yao, *J. Solid State Chem.* **2019**, *270*, 436.

[87] D. Yang, R. Yang, X. Ren, X. Zhu, Z. Yang, C. Li, S. F. Liu, *Adv. Mater.* **2016**, *28*, 5206.

[88] H. Cheng, Y. Li, M. Zhang, K. Zhao, Z. S. Wang, *ChemSusChem* **2020**, *13*, 2779.

[89] Q. Wu, W. Zhou, Q. Liu, P. Zhou, T. Chen, Y. Lu, Q. Qiao, S. Yang, *ACS Appl. Mater. Interfaces* **2016**, *8*, 34464−34473.

[90] D. Li, L. Chao, C. Chen, X. Ran, Y. Wang, T. Niu, S. Lv, H. Wu, Y. Xia, C. Ran, L. Song, S. Chen, Y. Chen, W. Huang, *Nano Lett.* **2020**, *20*, 5799.

[91] C. Geffroy, E. Grana, T. Bessho, S. Almosni, Z. Tang, A. Sharma, T. Kinoshita, F. Awai, E. Cloutet, T. Toupance, H. Segawa, G. Hadziioannou, *ACS Appl. Energy Mater.* **2020**, *3*, 1393.

[92] H. Zhang, Y. Shi, F. Yan, L. Wang, K. Wang, Y. Xing, Q. Dong, T. Ma, *Chem. Commun.* **2014**, *50*, 5020.

[93] N. Harindu Hemasiri, S. Kazim, L. Calio, S. Paek, M. Salado, G. Pozzi, L. Lezama, M. K. Nazeeruddin, S. Ahmad, *ACS Appl. Mater. Interfaces* **2020**, *12*, 9395.

[94] X. Zhou, M. Hu, C. Liu, L. Zhang, X. Zhong, X. Li, Y. Tian, C. Cheng, B. Xu, *Nano Energy* **2019**, *63*, 103866.

[95] H. M. Jian, H. Chen, L. He, C. J. Zhao, J. Chen, T. G. Jiu, G. H. Tao, *J. Electrochem. Soc.* **2021**, *168*, 036503.

[96] M. Elawad, H. Lee, Z. Yu, L. Sun, *Phys. B Condens. Matter* **2020**, *586*, 412124.

[97] S. Sonmezoglu, S. Akin, *Nano Energy* **2020**, *76*, 105127.

[98] R. Yuan, B. Cai, Y. Lv, X. Gao, J. Gu, Z. Fan, X. Liu, C. Yang, M. Liu, W.-H. Zhang, *Energy Environ. Sci.* **2021**, *14*, 5074.

[99]   Y. Yang, H. Lu, S. Feng, L. Yang, H. Dong, J. Wang, C. Tian, L. Li, H. Lu, J. Jeong, S. M. Zakeeruddin, Y. Liu, M. Grätzel, A. Hagfeldt, *Energy Environ. Sci.* **2021**, *14*, 3447.

[100]   Y. Zhao, Q. Ye, Z. Chu, F. Gao, X. Zhang, J. You, *Energy Environ. Mater.* **2019**, *2*, 93.

[101]   X. Zheng, Y. Hou, C. Bao, J. Yin, F. Yuan, Z. Huang, K. Song, J. Liu, J. Troughton, N. Gasparini, C. Zhou, Y. Lin, D.-J. Xue, B. Chen, A. K. Johnston, N. Wei, M. N. Hedhili, M. Wei, A. Y. Alsalloum, P. Maity, B. Turedi, C. Yang, D. Baran, T. D. Anthopoulos, Y. Han, Z.-H. Lu, O. F. Mohammed, F. Gao, E. H. Sargent, O. M. Bakr, *Nat. Energy* **2020**, *5*, 131.

[102]   Z. Luo, F. Wu, T. Zhang, X. Zeng, Y. Xiao, T. Liu, C. Zhong, X. Lu, L. Zhu, S. Yang, C. Yang, *Angew. Chemie Int. Ed.* **2019**, *58*, 8520.

[103]   M. Li, C. Zhao, Z. K. Wang, C. C. Zhang, H. K. H. Lee, A. Pockett, J. Barbé, W. C. Tsoi, Y. G. Yang, M. J. Carnie, X. Y. Gao, W. X. Yang, J. R. Durrant, L. S. Liao, S. M. Jain, *Adv. Energy Mater.* **2018**, *8*, 1801509.

[104]   X. Guo, X. Huang, J. Su, Z. Lin, J. Ma, J. Chang, Y. Hao, *Chem. Eng. J.* **2021**, *417*, 129184.

[105]   L. Calió, S. Kazim, M. Grätzel, S. Ahmad, *Angew. Chemie Int. Ed.* **2016**, *55*, 14522.

[106]   T. Bu, J. Li, H. Li, C. Tian, J. Su, G. Tong, L. K. Ono, C. Wang, Z. Lin, N. Chai, X. L. Zhang, J. Chang, J. Lu, J. Zhong, W. Huang, Y. Qi, Y. B. Cheng, F. Huang, *Science.* **2021**, *372*, 1327.

[107]   M. Saliba, S. Orlandi, T. Matsui, S. Aghazada, M. Cavazzini, J.-P. Correa-Baena, P. Gao, R. Scopelliti, E. Mosconi, K.-H. Dahmen, F. De Angelis, A. Abate, A. Hagfeldt, G. Pozzi, M. Graetzel, M. K. Nazeeruddin, *Nat. Energy* **2016**, *1*, 15017.

[108]   X. Huang, K. Wang, C. Yi, T. Meng, X. Gong, *Adv. Energy Mater.* **2016**, *6*, 1501773.

[109]   H. Luo, X. Lin, X. Hou, L. Pan, S. Huang, X. Chen, *Nano-Micro Lett.* **2017**, *9*, 39.

[110]   H. Zhang, H. Azimi, Y. Hou, T. Ameri, T. Przybilla, E. Spiecker, M. Kraft, U. Scherf, C. J. Brabec, *Chem. Mater.* **2014**, *26*, 5190.

[111]   R. C. Evans, A. G. Macedo, S. Pradhan, U. Scherf, L. D. Carlos, H. D. Burrows, *Adv. Mater.* **2010**, *22*, 3032.

[112]   H. Zhang, M. K. Nazeeruddin, W. C. H. Choy, *Adv. Mater.* **2019**, *31*, 1805702.

[113]   P. Schulz, D. Cahen, A. Kahn, *Chem. Rev.* **2019**, *119*, 3349.

[114] M. Vasilopoulou, A. Fakharuddin, A. G. Coutsolelos, P. Falaras, P. Argitis, A. R. B. M. Yusoff, M. K. Nazeeruddin, *Chem. Soc. Rev.* **2020**, *49*, 4496.

[115] M. Salado, A. D. Jodlowski, C. Roldan-carmona, G. De Miguel, *Nano Energy* **2018**, *50*, 220.

[116] X. Huang, H. Guo, K. Wang, X. Liu, *Org. Electron.* **2017**, *41*, 42.

[117] Z. Zhang, T. Guo, H. Yuan, L. Yu, R. Zhao, Z. Deng, J. Zhang, X. Liu, Z. Hu, Y. Zhu, *ACS Appl. Mater. Interfaces* **2021**, *13*, 727.

[118] X. Zhu, S. Yang, Y. Cao, L. Duan, M. Du, J. Feng, Y. Jiao, X. Jiang, Y. Sun, H. Wang, S. Zuo, Y. Liu, S. Liu, *Adv. Energy Mater.* **2022**, *12*, 2103491.

[119] M. Degani, Q. An, M. Albaladejo-Siguan, Y. J. Hofstetter, C. Cho, F. Paulus, G. Grancini, Y. Vaynzof, *Sci. Adv.* **2021**, *7*, eabj7930.

[120] D. Yang, X. Zhou, R. Yang, Z. Yang, W. Yu, X. Wang, C. Li, S. Liu, R. P. H. Chang, *Energy Environ. Sci.* **2016**, *9*, 3071.

[121] N. K. Noel, S. N. Habisreutinger, B. Wenger, Y. Lin, F. Zhang, J. B. Patel, A. Kahn, M. B. Johnston, H. J. Snaith, *Adv. Energy Mater* **2020**, *10*, 1903231.

[122] J. Xu, X. Shi, J. Chen, J. Luan, J. Yao, *J. Solid State Chem.* **2019**, *276*, 302.

[123] W. Chu, J. Yang, Q. Jiang, X. Li, J. Xin, *Appl. Surf. Sci.* **2018**, *440*, 1116.

[124] M. Stolterfoht, M. Grischek, P. Caprioglio, C. M. Wolff, E. Gutierrez-Partida, F. Peña-Camargo, D. Rothhardt, S. Zhang, M. Raoufi, J. Wolansky, M. Abdi-Jalebi, S. D. Stranks, S. Albrecht, T. Kirchartz, D. Neher, *Adv. Mater.* **2020**, *32*, 2000080.

[125] X. Lin, D. Cui, X. Luo, C. Zhang, Q. Han, Y. Wang, L. Han, *Energy Environ. Sci.* **2020**, *13*, 3823.

[126] H. Zhang, F. T. Eickemeyer, Z. Zhou, M. Mladenović, F. Jahanbakhshi, L. Merten, A. Hinderhofer, M. A. Hope, O. Ouellette, A. Mishra, P. Ahlawat, D. Ren, T. Sen Su, A. Krishna, Z. Wang, Z. Dong, J. Guo, S. M. Zakeeruddin, F. Schreiber, A. Hagfeldt, L. Emsley, U. Rothlisberger, J. V. Milić, M. Grätzel, *Nat. Commun.* **2021**, *12*, 3383.

[127] Z. Li, J. Dong, C. Liu, J. Guo, L. Shen, W. Guo, *Nano-Micro Lett.* **2019**, *11*, 50.

[128] X. Deng, L. Xie, S. Wang, C. Li, A. Wang, Y. Yuan, Z. Cao, *Chem. Eng. J.* **2020**, *398*, 125594.

[129] E. Y. Muslih, A. K. M. Hasan, L. Wang, *Chem. Eng. J.* **2021**, *411*, 128461.

[130] M. Anyi, L. Xiong, L. Linfeng, K. Zhiliang, L. Tongfa, R. Yaoguang, X. Mi, H. Min, C. Jiangzhao, Y. Ying, G. Michael, H. Hongwei, *Science.* **2014**, *345*, 295.

[131] P. Tiwana, P. Docampo, M. B. Johnston, H. J. Snaith, L. M. Herz, *ACS Nano* **2011**, *5*, 5158.

[132] J. P. Correa Baena, L. Steier, W. Tress, M. Saliba, S. Neutzner, T. Matsui, F. Giordano, T. J. Jacobsson, A. R. Srimath Kandada, S. M. Zakeeruddin, A. Petrozza, A. Abate, M. K. Nazeeruddin, M. Grätzel, A. Hagfeldt, *Energy Environ. Sci.* **2015**, *8*, 2928.

[133] J. Jeong, M. Kim, J. Seo, H. Lu, P. Ahlawat, A. Mishra, Y. Yang, M. A. Hope, F. T. Eickemeyer, M. Kim, Y. J. Yoon, I. W. Choi, B. P. Darwich, S. J. Choi, Y. Jo, J. H. Lee, B. Walker, S. M. Zakeeruddin, L. Emsley, U. Rothlisberger, A. Hagfeldt, D. S. Kim, M. Grätzel, J. Y. Kim, *Nature* **2021**, *592*, 381.

[134] R. Wang, M. Mujahid, Y. Duan, Z.-K. Wang, J. Xue, Y. Yang, *Adv. Funct. Mater.* **2019**, *29*, 1808843.

[135] T. A. Berhe, W. Su, C. Chen, C. Pan, J. Cheng, H. Chen, M. Tsai, L. Chen, A. A. Dubale, B. Hwang, *Energy Environ. Sci.* **2016**, *9*, 323.

[136] D. Wang, M. Wright, N. K. Elumalai, A. Uddin, *Sol. Energy Mater. Sol. Cells* **2016**, *147*, 255.

[137] R. Xia, X.-X. Gao, Y. Zhang, N. Drigo, V. I. E. Queloz, F. F. Tirani, R. Scopelliti, Z. Huang, X. Fang, S. Kinge, Z. Fei, C. Roldán-Carmona, M. K. Nazeeruddin, P. J. Dyson, *Adv. Mater.* **2020**, *32*, 2003801.

[138] Y. Wang, L. Chao, T. Niu, D. Li, Q. Wei, H. Wu, J. Qiu, H. Lu, C. Ran, Q. Zhong, L. Song, G. Xing, Y. Xia, Y. Chen, P. Müller-Buschbaum, W. Huang, *Sol. RRL* **2021**, *5*, 2000582.

[139] J. Wang, X. Ye, Y. Wang, Z. Wang, W. Wong, C. Li, *Electrochim. Acta* **2019**, *303*, 133.

[140] A. Wang, X. Deng, J. Wang, S. Wang, X. Niu, F. Hao, L. Ding, *Nano Energy* **2021**, *81*, 105631.

[141] S. Bai, P. Da, C. Li, Z. Wang, Z. Yuan, F. Fu, M. Kawecki, X. Liu, N. Sakai, J. T. W. Wang, S. Huettner, S. Buecheler, M. Fahlman, F. Gao, H. J. Snaith, *Nature* **2019**, *571*, 245.

[142] J. Du, Y. Wang, Y. Zhang, G. Zhao, Y. Jia, X. Zhang, Y. Liu, *Phys. Status Solidi - Rapid Res. Lett.* **2018**, *12*, 1800130.

[143] G. Li, Z. Su, M. Li, F. Yang, M. H. Aldamasy, J. Pascual, F. Yang, H. Liu, W. Zuo, D. Di Girolamo, Z. Iqbal, G. Nasti, A. Dallmann, X. Gao, Z. Wang, M. Saliba, A. Abate, *Adv. Energy Mater.* **2021**, *11*, 2101539.

[144] Y. H. Lin, N. Sakai, P. Da, J. Wu, H. C. Sansom, A. J. Ramadan, S. Mahesh, J. Liu, R. D. J. Oliver, J. Lim, L. Aspitarte, K. Sharma, P. K. Madhu, A. B. Morales-Vilches, P. K. Nayak, S. Bai, F. Gao, C. R. M. Grovenor, M. B. Johnston, J. G. Labram, J. R. Durrant, J. M. Ball, B. Wenger, B. Stannowski, H. J. Snaith, *Science.* **2020**, *369*, 96.

[145] S. Wang, B. Yang, J. Han, Z. He, T. Li, Q. Cao, J. Yang, J. Suo, X. Li, Z. Liu, S. (Frank) Liu, C. Tang, A. Hagfeldt, *Energy Environ. Sci.* **2020**, *13*, 5068.

[146] M. Salado, M. A. Fernández, J. P. Holgado, S. Kazim, M. K. Nazeeruddin, P. J. Dyson, S. Ahmad, *ChemSusChem* **2017**, *10*, 3846.

[147] R. Wang, J. Xue, L. Meng, J.-W. Lee, Z. Zhao, P. Sun, L. Cai, T. Huang, Z. Wang, Z.-K. Wang, Y. Duan, J. L. Yang, S. Tan, Y. Yuan, Y. Huang, Y. Yang, *Joule* **2019**, *3*, 1464.

[148] Y. Yuan, J. Chae, Y. Shao, Q. Wang, Z. Xiao, A. Centrone, J. Huang, *Adv. Energy Mater.* **2015**, *5*, 1500615.

[149] X. Li, M. Ibrahim Dar, C. Yi, J. Luo, M. Tschumi, S. M. Zakeeruddin, M. K. Nazeeruddin, H. Han, M. Grätzel, *Nat. Chem.* **2015**, *7*, 703.

[150] J. Yang, W. Sheng, R. Li, L. Gong, Y. Li, L. Tan, Q. Lin, Y. Chen, *Adv. Energy Mater.* **2022**, 2103652.

[151] Z. Xue, L. Qin, J. Jiang, T. Mu, G. Gao, *Phys. Chem. Chem. Phys.* **2018**, *20*, 8382.

[152] F. Philippi, T. Welton, *Phys. Chem. Chem. Phys.* **2021**, *23*, 6993.

[153] O. Y. Fajardo, F. Bresme, A. A. Kornyshev, M. Urbakh, *ACS Nano* **2017**, *11*, 6825.

Table of contents entry

F. Wang, D. Duan, M. Singh, C. M. Sutter-Fella, L. Li, P. Naumov, and H. Hu

Ionic Liquid Engineering in Perovskite Photovoltaics